NASA Contractor Report 172529

AERODYNAMIC-STRUCTURAL STUDY OF CANARD WING,
DUAL WING, AND CONVENTIONAL WING SYSTEMS
FOR GENERAL AVIATION APPLICATIONS

Bruce P. Selberg and Donald L. Cronin

UNIVERSITY OF MISSOURI-ROLLA
Rolla, Missouri

Grant NAG1-26
February 1985

National Aeronautics and
Space Administration

Langley Research Center
Hampton, Virginia 23665

TABLE OF CONTENTS

PERFORMANCE SUMMARY

An analytical aerodynamic structural airplane configuration study was conducted. The prescribed design specifications were for a high performance cruise mission of 563 km/hr (350 mi/hr) between the altitude of 9.44-12192 m (30-40,000 ft) with a range equal to or greater than 2414 km (1500 mi). Two airfoils were studied: the medium speed turbulent airfoil, NASA MS(1)-0313 and the natural laminar airfoil, NASA NL(S)-0715F, which has recently been given the official NASA designation of NLF-0215F. The design specifications required two separate baseline aircraft: a six-passenger single engine turboprop with a 5338 N (1200 lb) payload, shown in figure 1, and a twelve-passenger twin turbofan with a 10676 N (2400 lb) payload, shown in figure 2. In addition to the baseline configuration, six- and twelve-place canard configurations shown in figures 3 and 4 respectively, an aerodynamically closely coupled six- and twelve-place dual wing configuration shown in figures 5 and 6 respectively, and a swept forward swept rearward six- and twelve-place configuration shown in figures 7 and 8 respectively were also analyzed. The single wing and canard configurations which were not structurally joined together were limited to an aspect ratio, AR, between 6 and 12 and a wing loading, W/S, between 1197-2873 N/m^2 (25-60 lb/ft^2). No aspect ratio limit was placed on the configurations that were structurally connected. All configurations with the same payload utilized the same fuselage and internal components.

The aerodynamic analysis employed a two dimensional multi-element vortex panel program to accurately predict the inviscid aerodynamic coupling, with thickness taken into account. This was coupled to a momentum integral technique to predict boundary layer properties and drag with the Squire-Young formula. The output of the inviscid program, in terms of C_{ℓ_α} and C_{ℓ_0}, is used as input to a three dimensional vortex lattice program which predicts

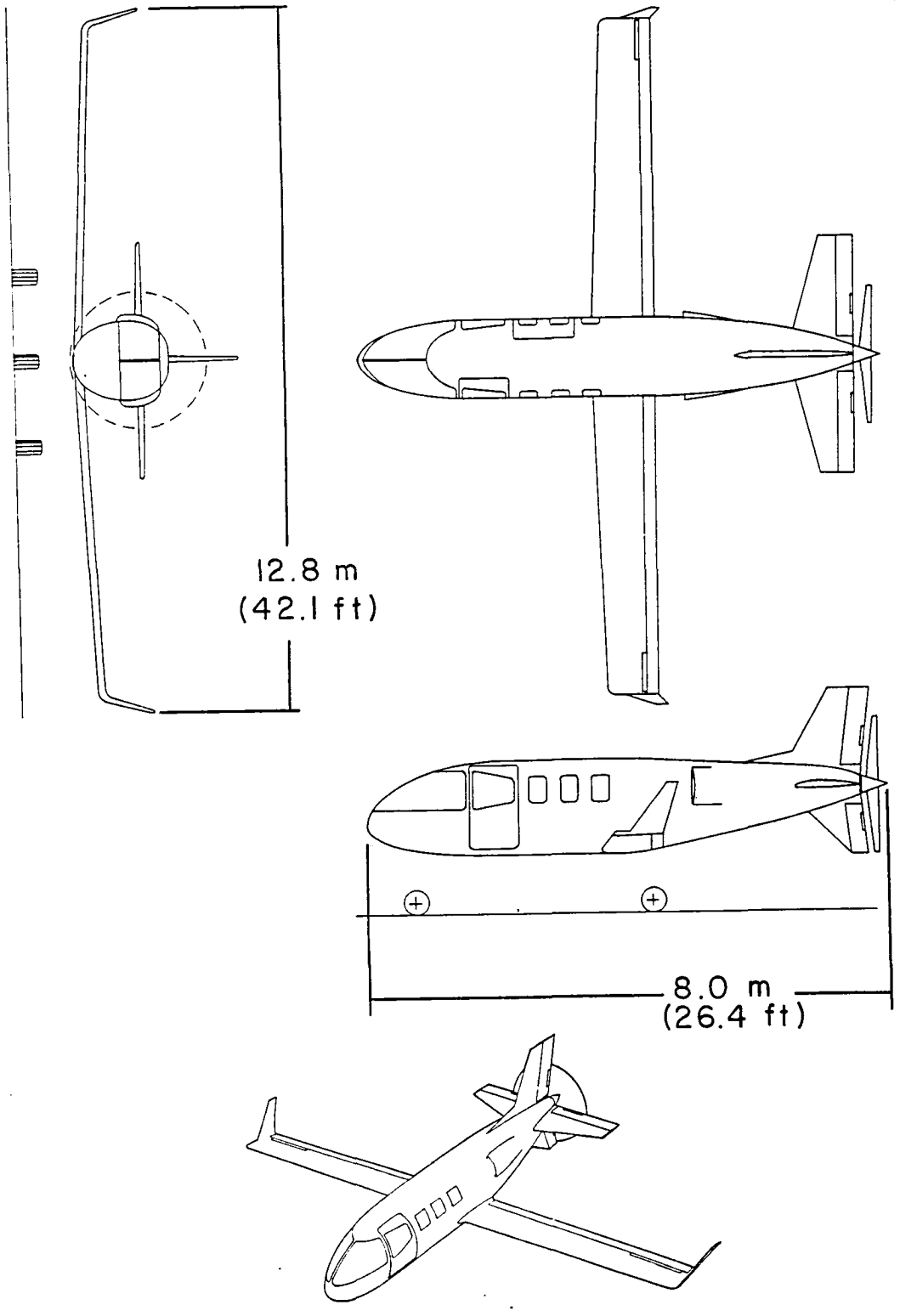

Figure 1. Six-Place Baseline Configuration.

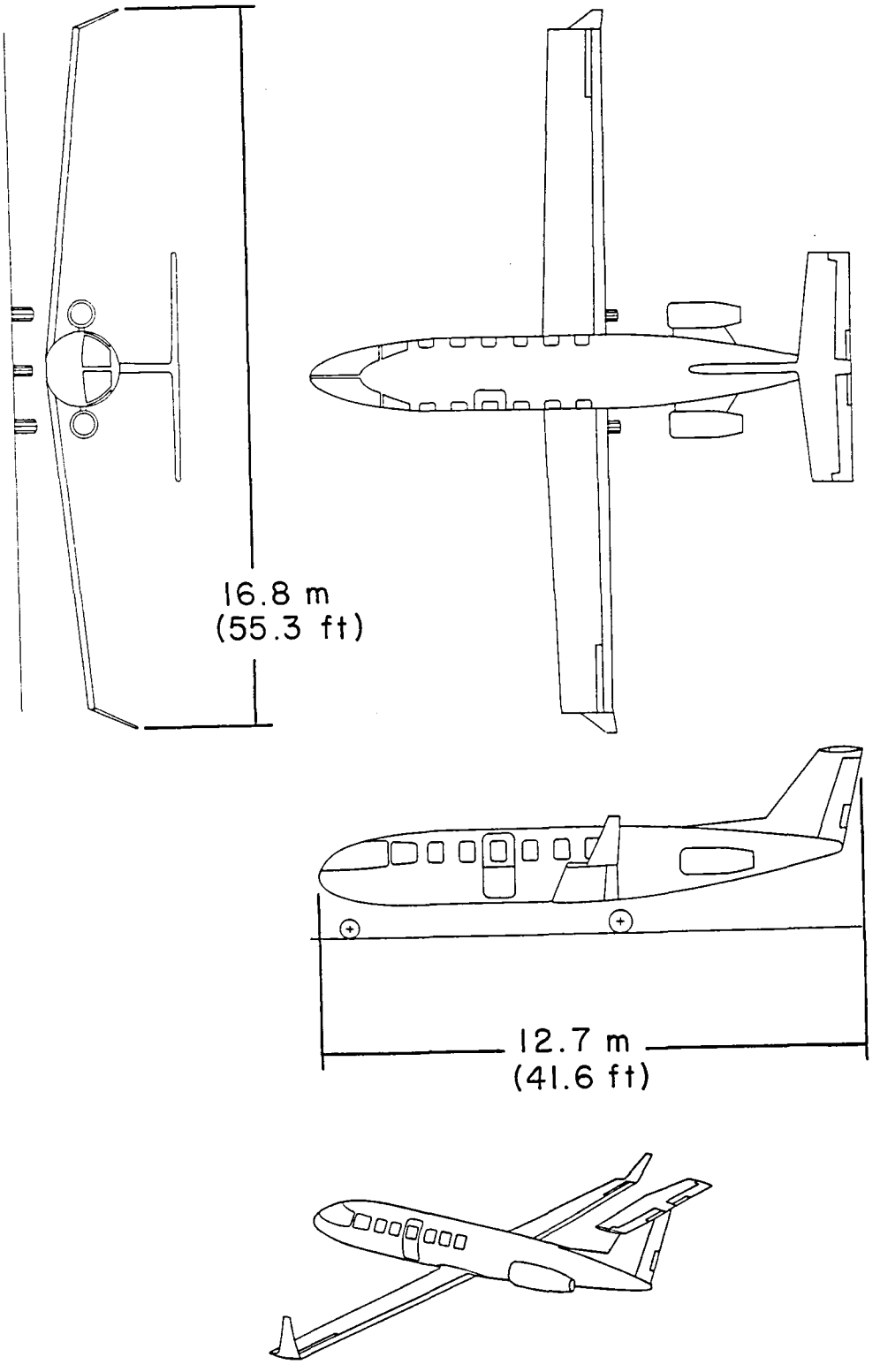

Figure 2. Twelve-Place Baseline Configuration.

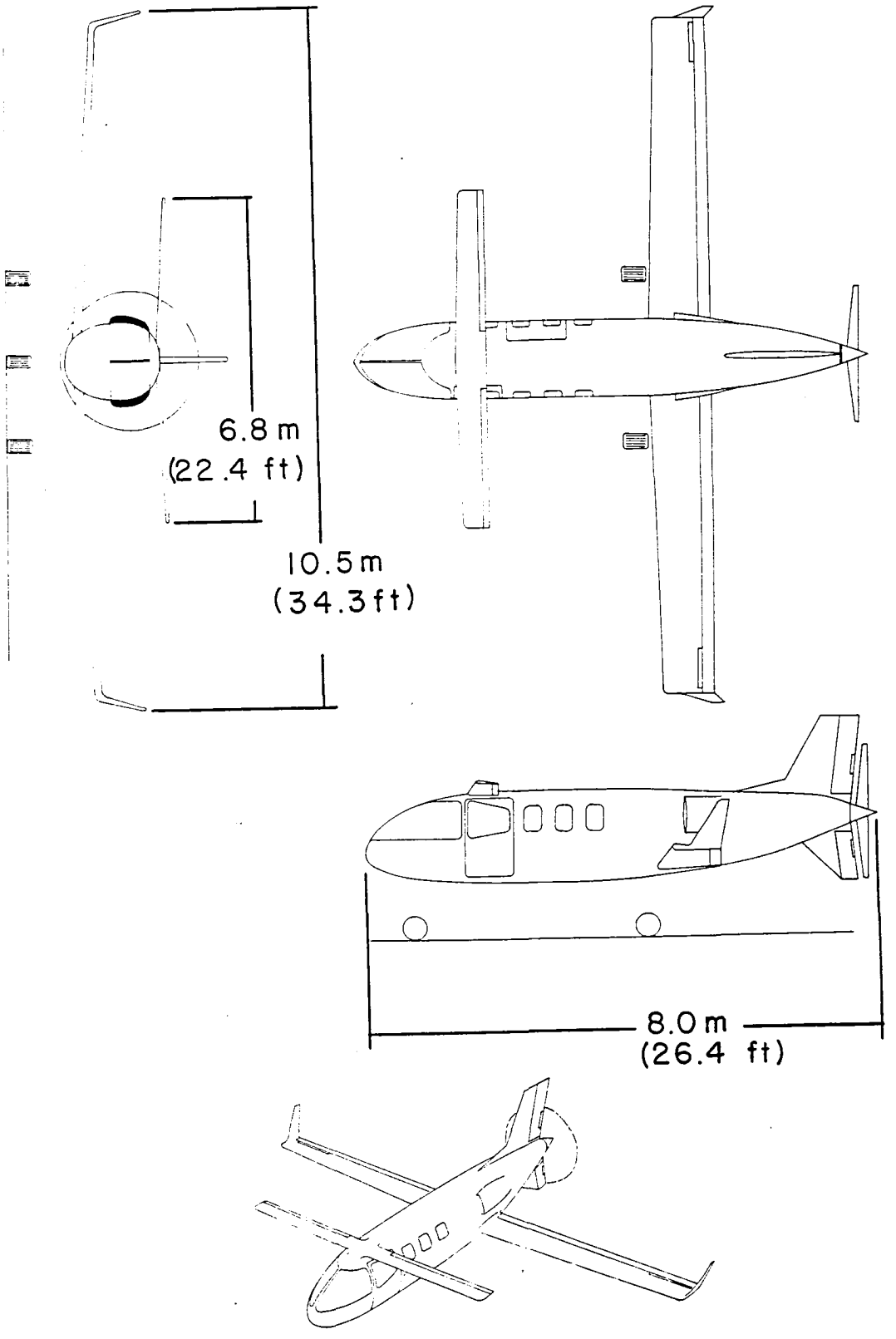

Figure 3. Six-Place Canard Configuration.

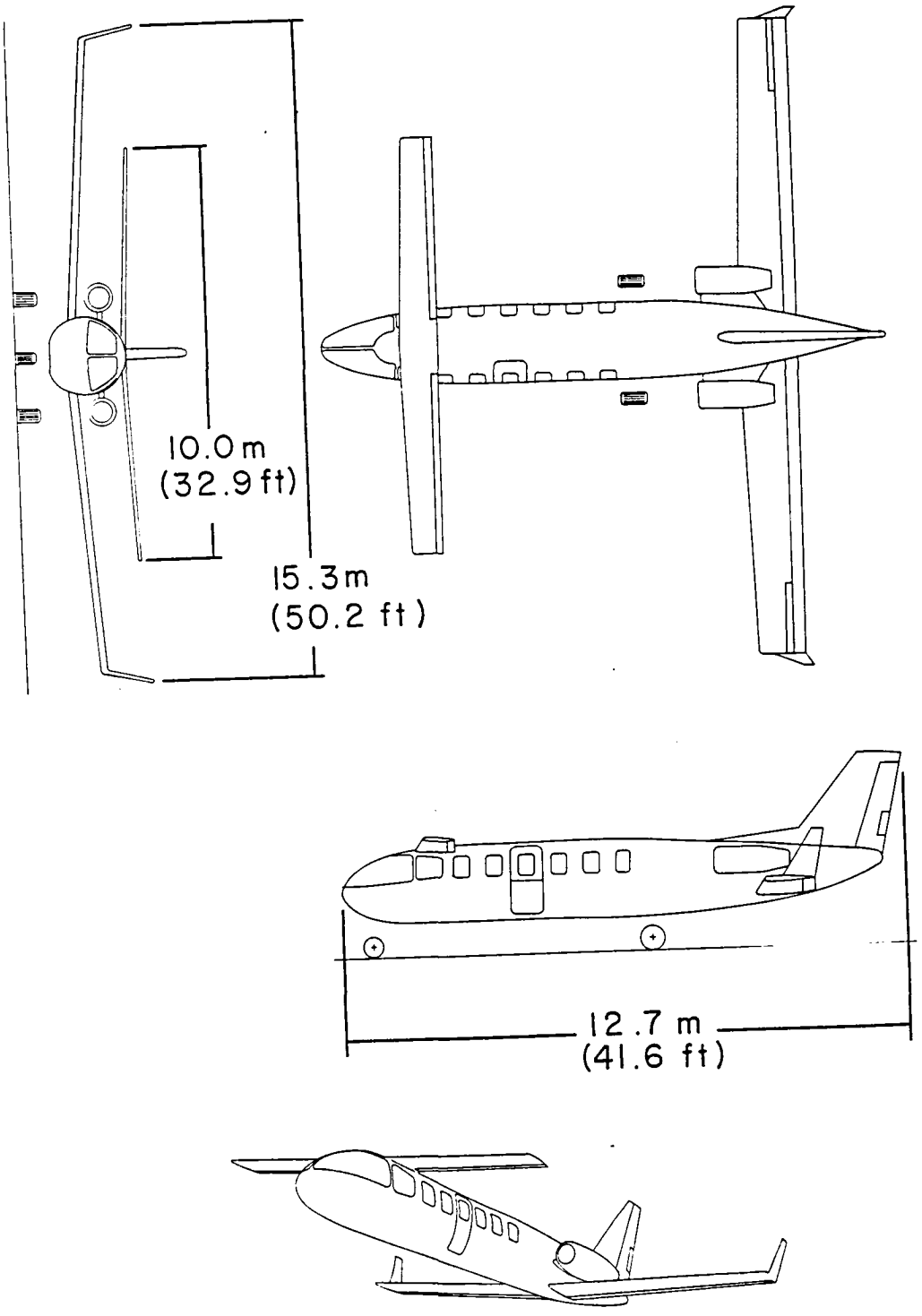

Figure 4. Twelve-Place Canard Configuration.

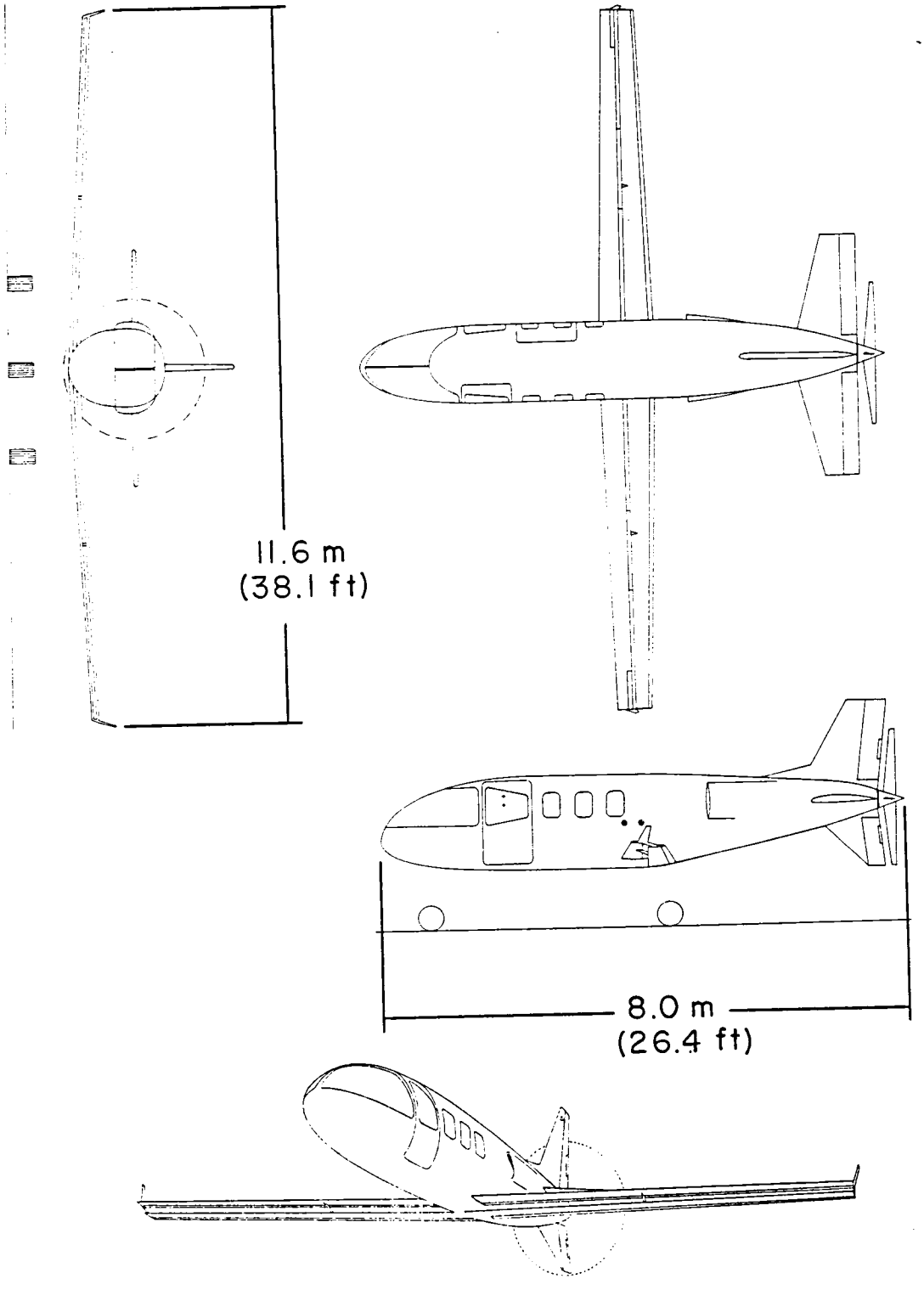

Figure 5. Six-Place Dual Wing Configuration.

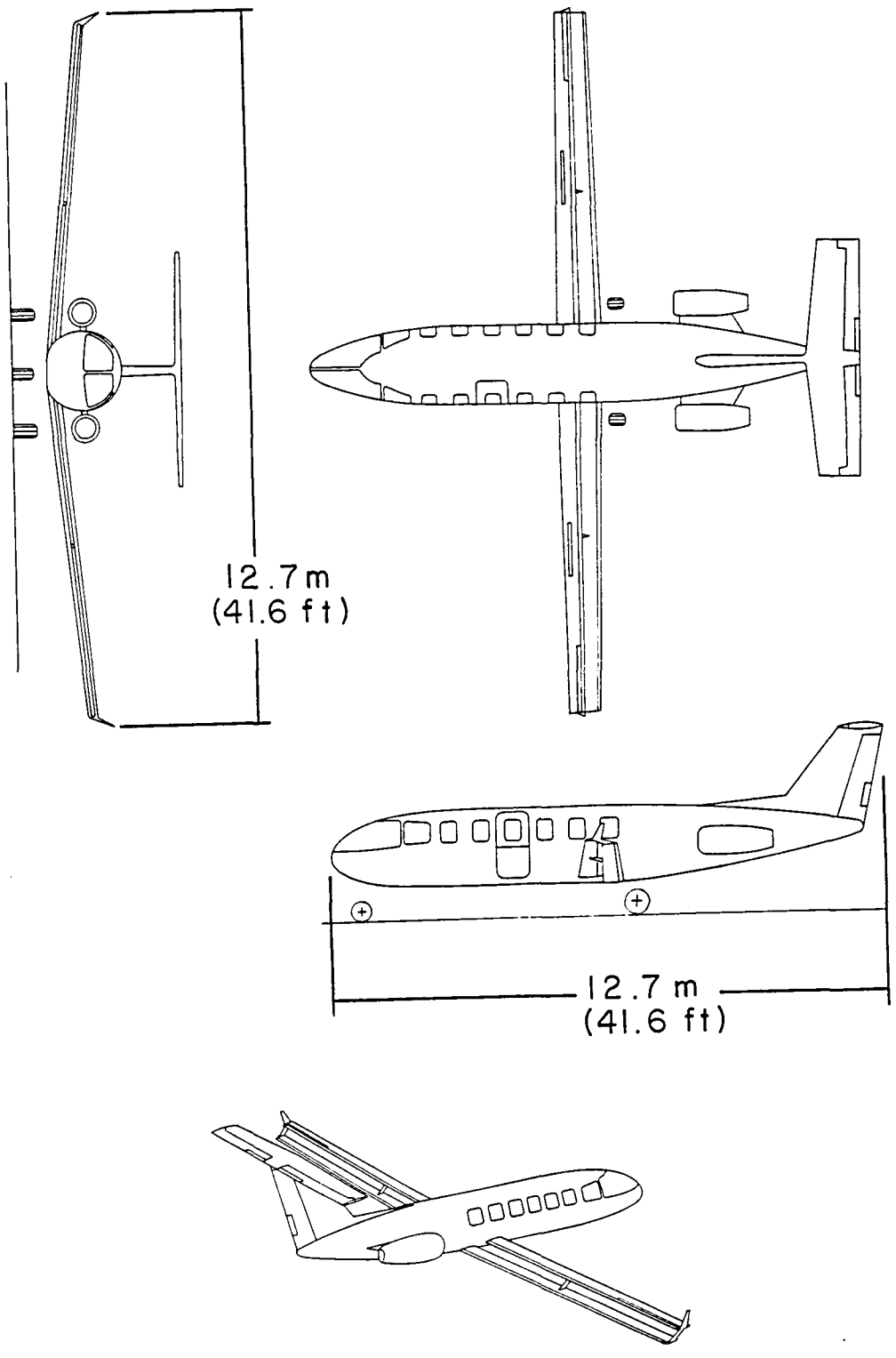

Figure 6. Twelve-Place Dual Wing Configuration.

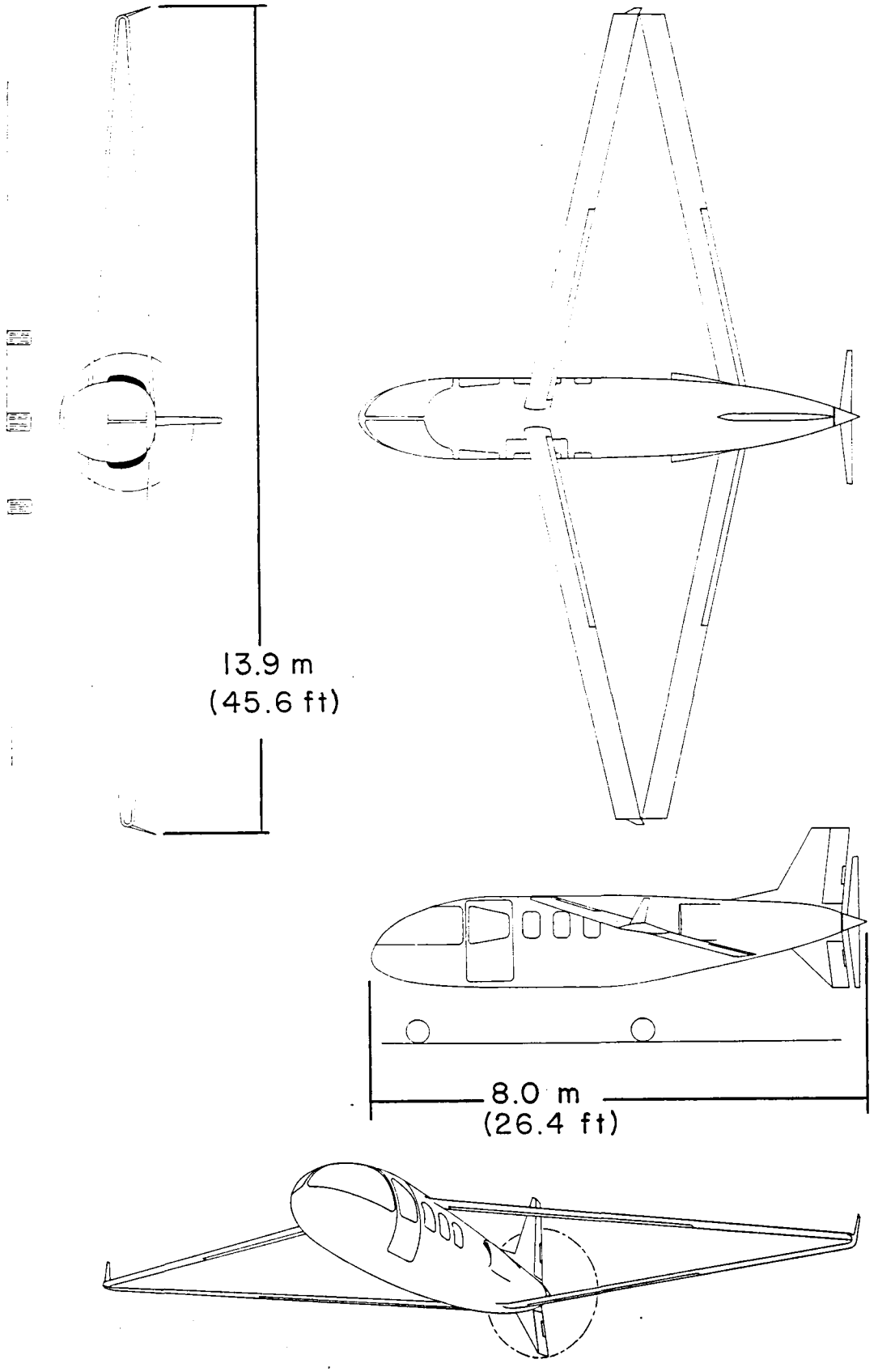

Figure 7. Six-Place Swept Forward Swept Rearward, SFSR, Configuration.

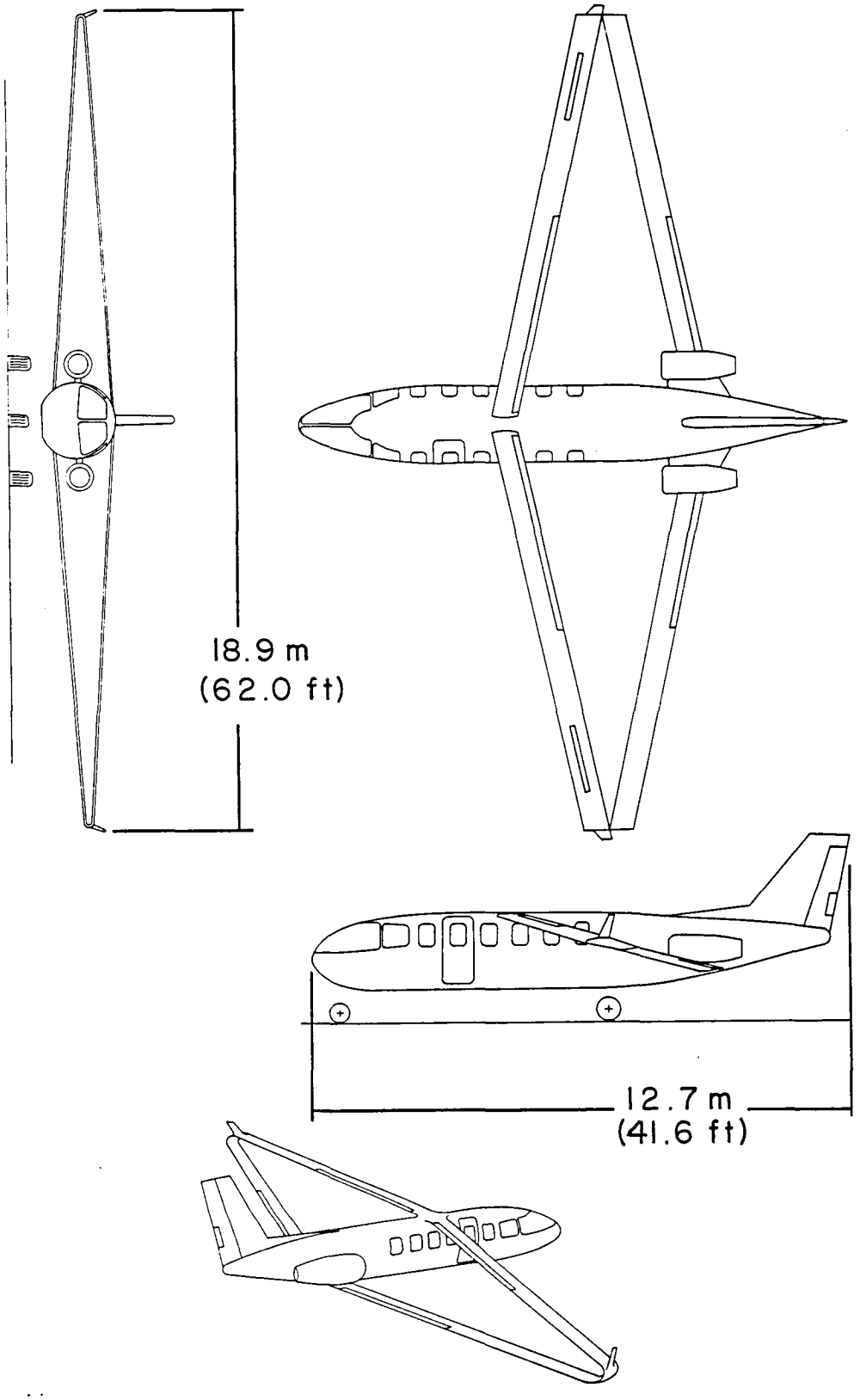

Figure 8. Twelve-Place Swept Forward Swept Rearward, SFSR, Configuration.

the span lift distribution and induced drag. These results are then fed into an optimization program along with weight equations and the minimum cruise drag is obtained.

The weight estimates utilize modified equations from Nicolai[1], Torenbeek [2,3], and a UMR design project[4]. Wing weight predictions are made from modified composite wing weight equations from Torenbeek, NASTRAN and SEMOBEAM optimization results for each configuration, and scaled NASTRAN results using a further modified Torenbeek formula[5].

The results shown in Tables 1 and 2 are trimmed 6-place and 12-place results using the modified Torenbeek wing weight formula and constant engine weight. For the six-place configuration only the dual wing and the SFSR wing aircraft offer reduced drag and hence increased range over the baseline. Both the canard configurations have higher drag and shorter ranges. For the twelve-place configurations the dual and SFSR configurations have increased ranges as well as the NLS-canard configuration.

The total wing weights as predicted by the modified Torenbeek wing weight formula over-predicted the weights of both the dual wing and the swept forward swept rearward configurations. Table 3 shows the weight comparisons of the total wing using the Torenbeek formula and the NASTRAN-SEMOBEAM results, with additional weights for leading edge, trailing edge, braces, and winglets. Since the dual wing weights using the Torenbeek formula are substantially greater than the NASTRAN weights, the quantitative comparisons between the dual configurations and the single wing configurations are in error. Tables 1 and 2, however, do give a valid comparison between the baseline and the canard configurations since the weight estimates are valid. When the NASTRAN-SEMOBEAM weights are used, along with variable engine weight sized to cruise drag requirements, and detailed weights for control surfaces, leading edges, winglets, and structural

TABLE 1.

TRIMMED 6-PLACE WITH WINGLETS - ENGINE WEIGHT CONSTANT

(Modified Torenbeek Weight Formula)

	W_{cr} N (lb)	W_{wing} N (lb)	$\frac{W_{wing}}{W_{baseline\ wing}}$	P_{req} kw (HP)	$\left(\frac{L}{D}\right)_{cr}$	$\frac{e}{e_{elliptical}}$	$\frac{W}{S}$ N/m^2 (lb_f/ft^2)	R km (mi)	$\frac{\Delta R}{R}$ %
MS(1)-0313									
SINGLE WING BASELINE	19,149 (4305)	1,868 (420)	1.0	159 (213)	18.9	0.86	1,502 (31.0)	2,778 (1726)	0.0
CANARD $S_w/S_c = \frac{70}{30}$	18,588 (4179)	1,564 (349)	0.83	170 (228)	17.1	0.72	1,415 (29.9)	2,590 (1609)	-6.8
DUAL WING	19,028 (4278)	1,739 (388)	0.92	145 (194)	19.7	0.92	2,592 (53.5)	2,913 (1810)	4.9
SFSR	19,620 (4411)	2,559 (571)	1.36	152 (203)	20.3	0.90	1,827 (37.7)	2,912 (1809)	4.8
NL(S)-0715F									
SINGLE WING	18,935 (4257)	1,644 (367)	0.87	152 (203)	19.6	0.84	1,652 (34.1)	2,913 (1810)	4.9
CANARD $S_w/S_c = \frac{80}{20}$	18,793 (4225)	1,769 (395)	0.94	154 (206)	19.2	0.81	1,022 (21.1)	2,876 (1787)	3.5
DUAL WING	19,295 (4338)	1,963 (438)	1.04	148 (199)	20.4	0.92	2,059 (42.5)	2,976 (1849)	7.1
SFSR	19,264 (4331)	2,178 (486)	1.16	139 (187)	21.6	0.88	2,355 (48.6)	3,157 (1961)	13.6

TABLE 2.

TRIMMED 12-PLACE WITH WINGLETS - ENGINE WEIGHT CONSTANT

(Modified Torenbeek Weight Formula)

	W_{cr} N (lb)	W_{wing} N (lb)	$\frac{W_{wing}}{W_{baseline\ wing}}$	P_{req} kw (HP)	$\left(\frac{L}{D}\right)_{cr}$	$\frac{e}{e_{elliptical}}$	$\frac{W}{S}$ N/m^2 (lb_f/ft^2)	R km (mi)	$\frac{\Delta R}{R}$ %
MS(1)-0313									
SINGLE WING BASELINE	38,182 (8584)	3,970 (886)	1.0	301 (403)	20.0	0.84	1,734 (35.8)	2,804 (1742)	0.0
CANARD $S_w/S_c = \frac{70}{30}$	37,123 (8346)	3,701 (826)	0.93	306 (410)	19.0	0.64	1,347 (27.8)	2,740 (1702)	-2.6
DUAL WING	38,658 (8691)	4,306 (961)	1.08	271 (363)	21.7	0.93	2,195 (45.3)	3,047 (1893)	8.4
SFSR	39,449 (8869)	5,238 (1169)	1.32	285 (382)	21.7	0.91	1,827 (37.7)	2,939 (1826)	4.5
NL(S)-0715F									
SINGLE WING	38,413 (8636)	4,060 (906)	1.02	278 (372)	21.6	0.86	1,492 (30.8)	3,007 (1868)	6.9
CANARD $S_w/S_c = \frac{80}{20}$	37,265 (8378)	3,397 (758)	0.86	275 (368)	21.3	0.69	1,158 (23.9)	3,049 (1894)	8.4
DUAL WING	39,498 (8880)	5,198 (1160)	1.31	272 (365)	22.7	0.96	1,831 (37.8)	3,073 (1909)	9.2
SFSR	38,760 (8714)	5,340 (1214)	1.37	259 (347)	23.4	0.88	2,200 (45.4)	3,224 (2003)	14.6

TABLE 3.

TOTAL WING WEIGHT COMPARISON

Configuration	MS(1)-0313 Total Wing Weight	
	Modified Torenbeek N (lb_m)	NASTRAN-SEMOBEAM N (lb_m)
BASELINE-6 PLACE	1,868 (420)	1,806 (406)
DUAL-6 PLACE	1,739 (388)	1,370 (319)
SFSR-6 PLACE	2,559 (571)	1,350 (338)
BASELINE-12 PLACE	3,970 (886)	2,953 (664)
DUAL-12 PLACE	8,691 (961)	3,065 (689)
SFSR-12 PLACE	5,238 (1,169)	2,904 (653)

ties, then the performance of the six- and twelve-place configurations are shown in Tables 4 and 5. For the six-place MS(1)-0313 configuration the dual wing and SFSR wing configurations have greater ranges, lower cruise drag, and lower total wing weight. The wing weights for the other dual wing cases are slightly higher with the ranges all 8-11 percent greater than the respective baselines. The SFSR configuration has ranges that are 12-20 percent greater than the respective baselines. All the NLS-0715 data were obtained using scaled NASTRAN-SEMOBEAM results via the Torenbeek equation.

If an all composite airplane is considered,then Tables 6 and 7 are the results for the 6- and 12-place configuration. Both the dual and the SFSR configurations have increased their range over the configurations that only had composite lifting surfaces. Figure 9 shows the specific range versus maximum cruise speed. The data points from within the box area are from this study. The other points are due to Kolhman and Holmes[6]. The integrated configuration includes an advanced rotary engine power plant which has excellent SFC values. If this engine is placed in the six-place configurations of this study, the dual composite rotary, dual CR, the SFSR composite rotary, SFSR CR, and the baseline composite rotary, baseline CR are the designated configurations. These configurations give range values significantly higher than the integrated configuration.

AERODYNAMIC SUMMARY

The results of the aerodynamic analysis revealed several interesting trends which are summarized below with respect to each of the configurations:

Baseline Aircraft

The baseline configurations achieved higher L/D ratios than current production airplanes. This is due to allowing larger aspect ratio, use of composite

TABLE 4.

TRIMMED 6-PLACE WITH WINGLETS

	W_{cr} N (lb)	W_{eng} N (lb)	W_{wing} N (lb)	$\frac{W_{wing}}{W_{baseline\ wing}}$	P_{req} kw (HP)	$\left(\frac{L}{D}\right)_{cr}$	$\frac{e}{e_{elliptical}}$	$\frac{W}{S}$ N/m^2 (lb_f/ft^2)	R km (mi)	$\frac{\Delta R}{R}$ %
MS(1)-0313										
SINGLE WING* BASELINE	19,673 (4423)	3483 (783)	1806 (406)	1.0	159 (213)	19.28	0.86	1,534 (31.6)	2,757 (1713)	
DUAL WING*	18,997 (4271)	3260 (733)	1419 (319)	0.79	148 (198)	20.13	0.92	2,461 (50.8)	2,981 (1852)	8.1
SFSR*	19,300 (4339)	3154 (709)	1503 (338)	0.83	142 (190)	21.23	0.90	1,831 (37.8)	3,095 (1923)	12.3
NL(S)-0715F										
SINGLE WING+ BASELINE	19,091 (4292)	3363 (756)	1383 (311)	0.77	152 (204)	19.66	0.84	1,710 (35.3)	2,899 (1801)	5.4
DUAL WING+	19,197 (4316)	3260 (733)	1548 (348)	0.86	148 (198)	20.39	0.92	2,093 (43.2)	2,983 (1853)	8.2
SFSR+	18,414 (4140)	3047 (685)	1245 (280)	0.69	136 (182)	21.32	0.88	2,355 (48.6)	3,231 (2007)	17.2

*NASTRAN Weights

+Scaled NASTRAN Weights

TABLE 5.

TRIMMED 12-PLACE WITH WINGLETS

	W_{cr} N (lb)	W_{eng} N (lb)	W_{wing} N (lb)	$\frac{W_{wing}}{W_{baseline\ wing}}$	P_{req} kw (HP)	$\left(\frac{L}{D}\right)_{cr}$	$\frac{e}{e_{elliptical}}$	$\frac{W}{S}$ N/m^2 (lb_f/ft^2)	R km (mi)	$\frac{\Delta R}{R}$ %
MS(1)-0313										
SINGLE WING* BASELINE	33,707 (7578)	3,754 (844)	2,953 (664)	1.0	281 (376)	18.79	0.84	1,720 (35.5)	2,971 (1846)	
DUAL WING*	33,671 (7570)	3,607 (811)	3,065 (689)	1.04	256 (343)	20.45	0.93	2,137 (44.1)	3,250 (2019)	9.4
SFSR*	32,941 (7406)	3,572 (803)	2,904 (653)	0.98	250 (335)	21.71	0.90	1,735 (35.8)	3,467 (2154)	16.7
NL(S)-0715F										
SINGLE WING+ BASELINE	33,458 (7522)	3,736 (840)	2,722 (612)	0.92	279 (374)	18.71	0.84	1,720 (35.5)	2,989 (1857)	0.5
DUAL WING+	33,778 (7594)	3,589 (807)	3,189 (717)	1.08	253 (339)	20.83	0.96	1,836 (37.9)	3,306 (2054)	11.3
SFSR+	32,453 (7296)	3,483 (783)	2,504 (563)	0.85	235 (315)	21.65	0.88	2,233 (46.1)	3,565 (2215)	20.0

*NASTRAN Weights

+Scaled NASTRAN Weights

TABLE 6.

TRIMMED 6-PLACE WITH WINGLETS

	W_{cr} N (lb)	W_{eng} N (lb)	W_{wing} N (lb)	$\frac{W_{wing}}{W_{baseline\ wing}}$	P_{req} kw (HP)	$\left(\frac{L}{D}\right)_{cr}$	$\frac{e}{e_{elliptical}}$	$\frac{W}{S}$ N/m^2 (lb_f/ft^2)	R km (mi)	$\frac{\Delta R}{R}$ %
MS(1)-0313										
SINGLE WING* BASELINE	19,673 (4423)	3,483 (783)	1,806 (406)	1.0	159 (213)	19.28	0.86	1,531 (31.6)	2,757 (1713)	
SINGLE WING#	17,187 (3864)	3,296 (741)	1,370 (308)	0.76	149 (200)	18.20	0.86	1,516 (31.3)	2,983 (1853)	8.2
DUAL WING#	16,880 (3795)	3,109 (699)	1,250 (281)	0.69	139 (187)	19.01	0.93	2,447 (50.5)	3,171 (1970)	15.0
SFSR#	16,524 (3715)	2,953 (664)	1,317 (296)	0.73	131 (176)	19.83	0.91	1,807 (37.3)	3,380 (2100)	22.6
NL(S)-0715F										
SINGLE WING++ BASELINE	17,294 (3888)	3,229 (726)	1,543 (347)	0.85	145 (195)	18.80	0.88	1,618 (33.4)	3,062 (1902)	11.0
DUAL WING++	16,991 (3820)	3,109 (699)	1,361 (306)	0.75	139 (187)	19.22	0.92	2,030 (41.9)	3,186 (1979)	15.5
SFSR++	16,564 (3724)	3,064 (691)	1,361 (247)	0.61	137 (185)	20.15	0.88	2,345 (48.6)	3,426 (2128)	24.2

*NASTRAN Weights

#All Composite, NASTRAN Wing Weights

++All Composite, Scaled NASTRAN Wing Weights

TABLE 7.

TRIMMED 12-PLACE WITH WINGLETS

	W_{cr} N (lb)	W_{eng} N (lb)	W_{wing} N (lb)	$\frac{W_{wing}}{W_{baseline\ wing}}$	P_{req} kw (HP)	$\left(\frac{L}{D}\right)_{cr}$	$\frac{e}{e_{elliptical}}$	$\frac{W}{S}$ N/m^2 (lb_f/ft^2)	R km (mi)	$\frac{\Delta R}{R}$ %
MS(1)-0313										
SINGLE WING* BASELINE	33,707 (7578)	3,754 (844)	2,953 (664)	1.0	281 (376)	18.79	0.84	1,715 (35.4)	2,971 (1846)	
SINGLE WING	29,904 (6723)	3,643 (819)	2,598 (584)	0.88	263 (352)	17.83	0.85	1,638 (33.8)	3,181 (1976)	7.0
DUAL WING#	29,824 (6705)	3,545 (797)	2,615 (588)	0.88	245 (328)	19.14	0.93	2,418 (49.9)	3,417 (2123)	15.1
SFSR#	29,094 (6541)	3,447 (775)	2,517 (566)	0.85	227 (304)	19.92	0.91	1,836 (37.9)	3,668 (2279)	23.5
NL(S)-0715F										
SINGLE WING++ BASELINE	29,721 (6682)	3,576 (804)	2,615 (558)	0.84	246 (330)	18.83	0.86	1,570 (32.4)	3,390 (2106)	14.1
DUAL WING++	29,979 (6740)	3,523 (792)	2,793 (628)	0.95	240 (322)	19.48	0.94	1,831 (37.8)	3,470 (2156)	16.8
SFSR++	28,778 (6470)	3,242 (730)	2,188 (492)	0.74	221 (297)	20.34	0.88	2,228 (46.0)	3,409 (2118)	14.7

*NASTRAN Weights

#All composite, NASTRAN Wing Weights

++All composite, Scaled NASTRAN Wing Weights

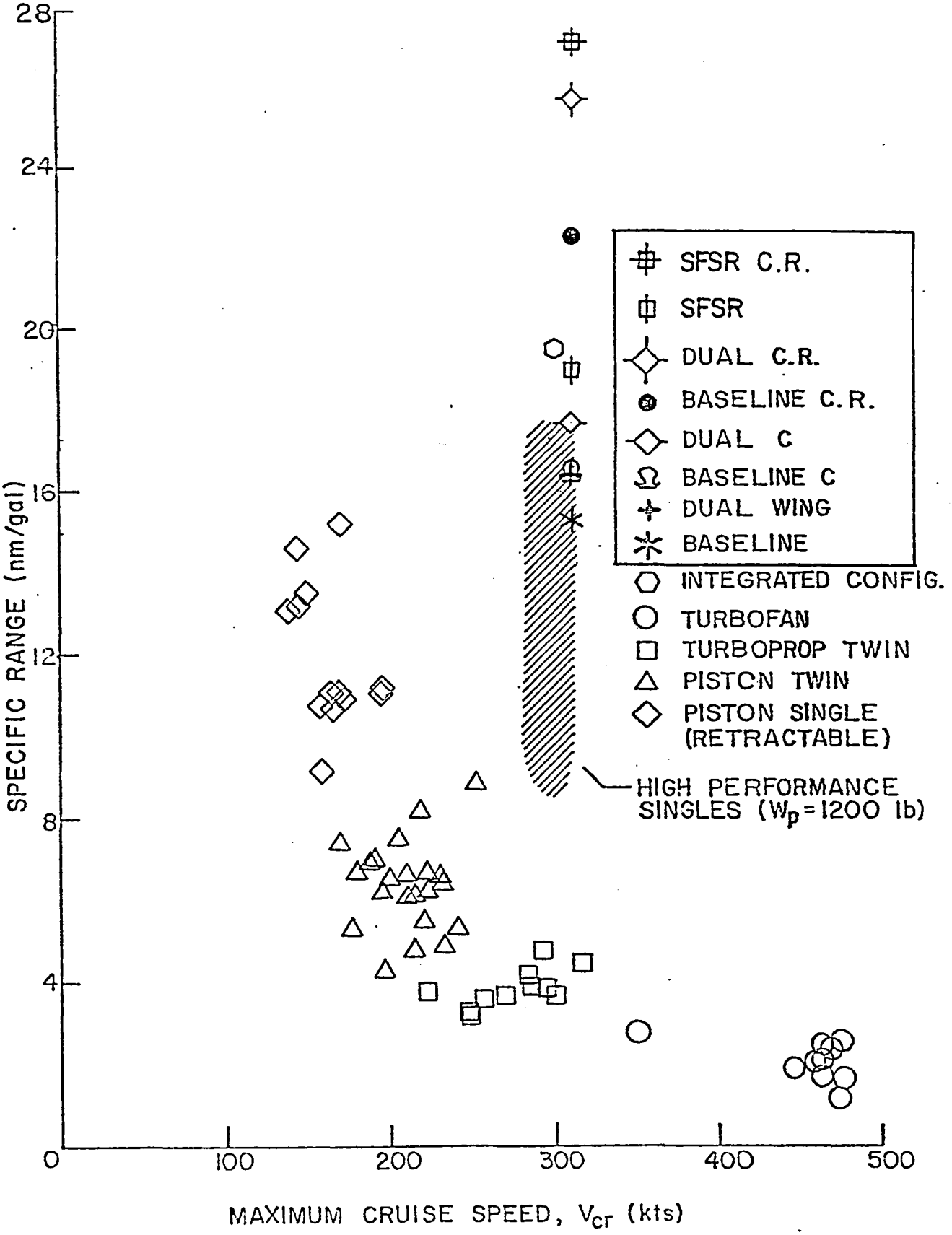

Figure 9. Specific Range Comparisons.

materials, permitting higher wing loadings, and using natural transition in the analysis thereby simulating new technology fabrication materials and techniques.

Canard Aircraft

The L/D ratios of the canard were below those of the baseline configurations. This was due to the trim drag penalty and the lower span efficiency. However, for non-optimum loading conditions the canard became superior to the baseline. For equal gross weights the canard is superior to the baseline. Moreover, the canard design can be made such that the wing is stall proof and hence the canard configuration would not be spinnable.

Dual Wing Aircraft

The dual wing aircraft consistently had higher L/D ratios than the baseline. This was due to a shifting of the two dimensional drag bucket to higher lift coefficient values thereby permitting higher cruise lift coefficients for the same two dimensional drag. The induced drag of the dual wing was also below that of the baseline with the dual wing having the highest span efficiency of all the configurations. The dual wing was penalized because it had to operate at Reynolds numbers that were almost an order of magnitude below the design airfoil Reynolds number. Operation at higher Reynolds numbers would have allowed two dimensional drag results that are below the single airfoil, at twice the Reynolds number for a wide range of lift coefficients; see dual wing section for details. Also if the dual wing configuration had used airfoils designed for the dual airfoil mode of operation, the L/D ratios would also have been higher.

Swept Forward Swept Rearward Aircraft

The swept forward swept rearward configurations also consistently had higher L/D ratios than the baseline configurations. This is attributable to lower induced drags and an absence of an extra horizontal control surface. The span efficiencies of the SFSR configurations were the second highest. However, the SFSR configuration may also not be adequately represented in that lateral stability was not investigated. A lateral stability analysis may require

changing dihedral angles as well as increasing vertical tail size to achieve stability. This would tend to lower the L/D.

None of the above designs considered optimum fuselages either in terms of drag or structures. Nor were the configurations optimized for the same wing area or the same maximum gross weight. Most of the above further constraints would benefit either the dual, SFSR, and the canard configurations.

STRUCTURES SUMMARY

At the start of the present study it was recognized that the main effort in structural analysis should be concentrated on the estimation of weight for the wing systems of current interest. Formulas available for the weight estimation of conventional monoplane wings, however manipulated or adjusted, could not be said to be appropriate for the task. A series of programs, PREPROCESSOR, NASTRAN, BIFORCE, and BISTRESS which incorporates SEMOBEAM, were utilized to design the wing system structurally to safely react limiting loads, to optimize the structure subject to the constraint that it remain viable for the specified loading, and then to estimate its weight. Baseline, dual, and swept forward swept rearward configurations, both six-place and twelve-place, were analyzed so that the relative weight advantage associated with the dual wing system of interest could be observed and objectively discussed.

All of the dual wing configurations produced during this study for the six-place aircraft are significantly lighter than the six-place conventional wing, the swept forward swept rearward wing system offers a 17 percent weight reduction over the baseline while the dual wing offers a 21 percent weight reduction over the baseline. Concerning what are considered to be the least subjective results, structural box weights, all dual wing configurations offer quite significant weight reduction possibilities relative to the conventional wing,

30 percent for the dual wing and 23 percent for the swept forward swept rearward wing configuration.

The twelve-place wing design utilized the same structural box layout as the six-place. However, since the chord was larger, this lowered the permissible buckling stress in the design process producing higher weights. Even using the same structural box, the dual wing is 70 pounds lighter than the baseline while the swept forward swept rearward is 33 pounds lighter than the baseline. Redesign of the structural boxes for both the twelve-place dual wing configurations and a modification to the weight estimation procedure will result in larger weight reductions for the twelve-place dual wing configurations relative to the twelve-place conventional wing.

In summary, for the present applications it appears possible to build a relatively light dual wing system in either aluminum or composite material. These dual wing systems appear to perform adequately from the standpoints of both statics and dynamics. The design of these systems will be more complicated -- requiring, even in the preliminary stages, more computer analysis and less reliance on proven formulas and established strategies. Based upon the present results it is concluded that the additional complexity -- both in terms of structure and design -- is worthwhile.

AERODYNAMICS

Methodology and Baseline Results

The high performance design specifications are given in Table 8. The specifications called for two baseline aircraft, a six-place turboprop personal aircraft, and a twelve-place turbofan business aircraft.

The fuselage cabins of both the six- and twelve-place aircraft were sized to present minimum frontal area, to reduce form drag, while providing necessary interior

Table 8

Parameter	Range of Values
Cruise Velocity - V_{CR}	563 km/hr (350 m/hr)
Cruise Range - R	2414 km (1500 mm)
Cruise Payload - Wt_{CR}	
six place	5338 N (1200 lb_m)
twelve place	10,676 N (2400 lb_m)
Wing Loading - W/S	1197-2873 W/m^2 (25-60 lb_f/ft^2)
Aspect Ratio	
single wing & canard	6-12
dual wings	no limit
Altitude Range	9144-12192 m (30-40 k ft)
Airfoil Sections	NLF-0715F (natural laminar flow airfoil) MS1-0313 (medium speed turbulent airfoil)

volume for the pilot, passengers, and baggage. Both cabins were designed to accommodate 95 percentile men. The width of the twelve-place fuselage was also influenced by the requirement to have a 30.5 cm (12 inch) aisle between the seats. The seat pitch for both versions was 91.4 cm (36 inches), except for the front row of seats which had a 111.7 cm (44 inch pitch). Each cabin was designed for a pressure altitude 2438 m (8000 ft) for the cruise altitude of 12192 m (40,000 ft).

The six-place cabin which is 132 cm (50 inches) high, 112 cm (44 inches) wide, and 4.42 m (14.5 ft) long, contains six seats in three rows of two seats each and has the baggage compartment aft of the last row of seats. The baggage compartment has an approximate volume of 0.82 m^3 (29 ft^3). The fuselage was designed for a retractable tricycle landing gear, the nose gear housed below and forward of the pressure cabin, and the main gear retracting below and aft of the baggage compartment. The main landing gear width is 2.62 m (8.6 ft) and exceeds the FAR overturning criterion. The single turboprop engine is located in the aft-most section of the fuselage tail cone, and has air inlets and exhausts on either side of the fuselage with the propeller shaft extending through the aft fuselage. The avionics and the environmental control unit were also housed in the fuselage aft of the pressure cabin. Entrance to the cabin compartment is through two doors, one on each side of the fuselage. One smaller door is located on the left which accesses the first row of seats, and a larger door is located on the right which accesses the two aft rows of seats. Both doors split in the middle and contain steps in the bottom half.

The twelve-place fuselage is very similar to the six, except it has two turbofan engines mounted on horizontal pylons which are attached to the aft section, and the cabin is considerably larger. The internal cabin dimensions are: 152 cm (60 inches) in height, 163 cm (64 inches) in width, and 7.37 m (24.2 ft) in length. The baggage compartment is located behind the last row of seats and is approximately 1.7 m^3 (60 ft^3) in volume. The retractable

tricycle landing gear is located in the same relative position as the landing gear for the six-place aircraft. The FAR overturning criterion was met with the same main gear width of 2.62 m (8.6 ft). Just as with the six-place aircraft, the avionics and environmental control unit were placed in the aft fuselage behind the baggage compartment. Entrance to the cabin is through a single mid-located split door on the left side of the fuselage.

The six-place aircraft uses a scaled version of the Pratt and Whitney PT6A-45A turboprop engine[7] with a 2.29 m (90 inch) diameter four-bladed propeller. Specific fuel consumption was assumed to be constant at 0.344 kg/hW-hr (0.55 lb/hp-hr). The engine weight was scaled by the ratio of required power to production power. The twelve-place aircraft uses two turbofan engines scaled from a General Aviation Turbine Engine (GATE) study[8], while assuming a 0.061 kg/N-hr (0.6 lb/lb-hr) thrust specific fuel consumption. The turbofan engine weights were scaled by the ratio of required thrust to reference engine thrust.

The aircraft weights were estimated with the aid of equations given by Nicolai[1] and Torenbeek[2,3] and from a UMR design project[4], a four-place high speed general aviation aircraft that utilized NASTRAN prediction methods.

The fuselage and empennage weights were determined for the six- and twelve-place aircraft by using Nicolai's equations[1] with the UMR four-place design as a reference aircraft[4]. Nicolai's equations were used as scaling factors on the reference weights by accounting for the different fuselage dimensions, take-off weights, and other important factors. The scale factors used were the average for commercial subsonic aircraft and light utility aircraft. Wing weights were estimated from a modification of Torenbeek's formula to account for composite wings which were used on both aircraft designs and from NASTRAN SEMOBEAM results. These modified composite wing weight formulas were checked against the results of a NASA internal memo[9] and showed good agreement. An ultimate

load factor of 5.7 was used and was calculated from a 3.8 g load with a factor of safety of 1.5. Weights of landing gear, avionics, electrical and fuel systems, and other equipment on board were estimated with Nicolai's equations. The weight of the required fuel was obtained by estimating take-off and climb fuel consumption, cruise fuel consumption for a range of 2414 km (1500 miles), descent and approach fuel consumption, and allowing for 20 percent fuel reserves.

The aerodynamic investigation was completed by using an inviscid vortex panel multi-element program[10] which was coupled to a momentum integral boundary layer analysis program[10]. These predicted theoretical two-dimensional inviscid and inviscid data. The results of the two-dimensional vortex panel analysis were used as input to a three-dimensional vortex lattice program to predict the induced drag of the finite lifting surface.

The laminar flow portion of the momentum integral program uses Thwaites' method[11] with Michel's transition criterion[12]. The turbulent flow solution is obtained by Head's momentum integral method[13] with the two-dimensional drag being calculated by the Squire-Young formula[14]. To check the validity of the predicted two-dimensional drag, the analytical results were compared to experimental results[15,16] known at the same Reynolds number for smooth airfoils. Figure 10 compares the theoretical to the experimental data for the MS(1)-0313 airfoil at a Reynolds number, R_c, of 4×10^6 and for the NL(S)-0715 airfoil at a Reynolds number of 6×10^6. This good agreement was achieved by using a Young's factor of 2.4 for the MS(1)-0313 and a Young's factor of 2.2 for the NL(S)-0715F in the Squire-Young equation. The same good agreement was obtained for both airfoils at other Reynolds numbers.

The vortex lattice program used on this study was developed at the University of Missouri-Rolla (UMR). It uses C_{ℓ_α} and C_{ℓ_0} values from the vortex panel program as input and predicts higher values of induced drag than

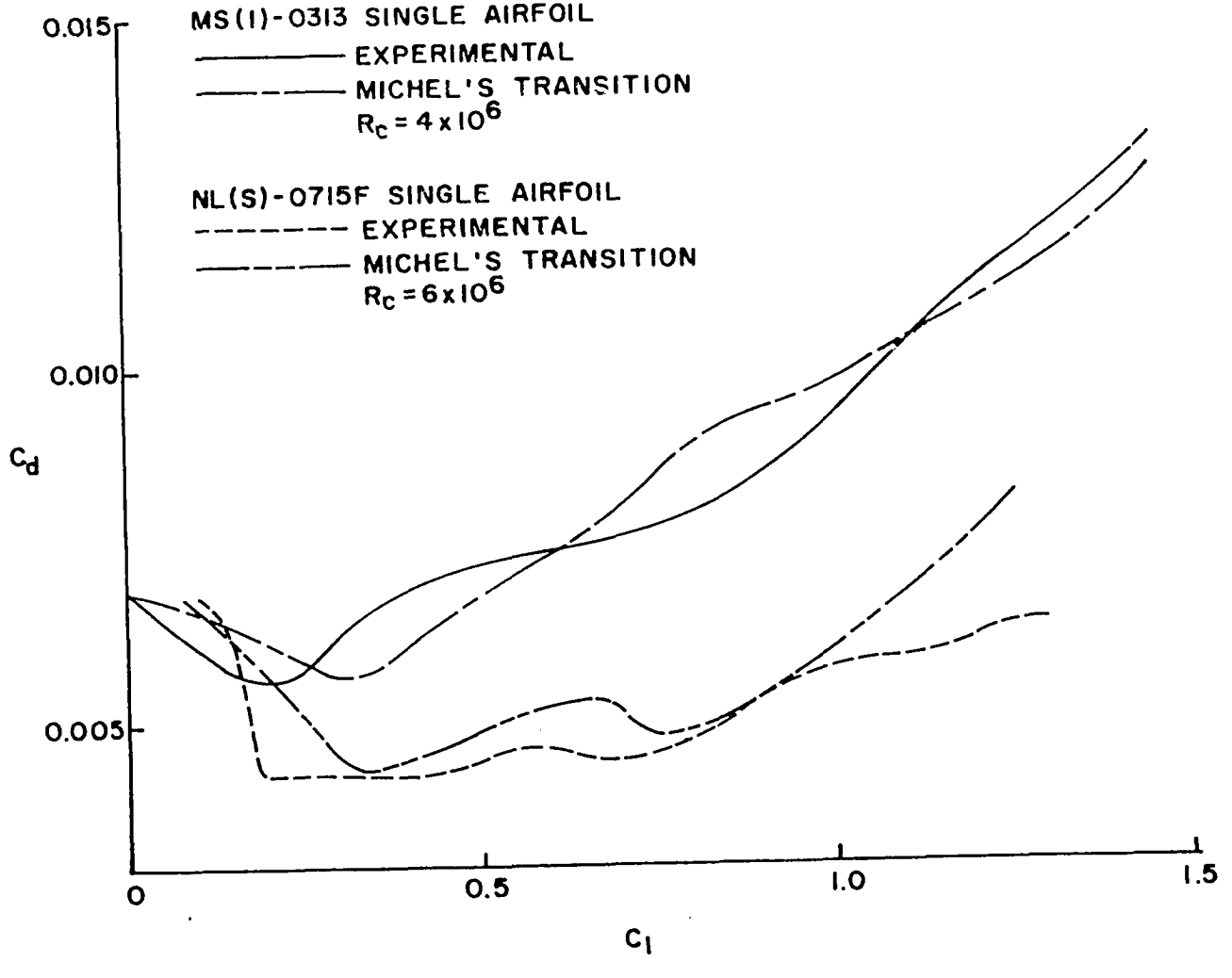

Figure 10. Two Dimensional Drag Results.

does a vortex lattice program, NARUVLE, developed by Tulinius[17], which underestimates induced drag[18]. Figure 11 presents a wing fuselage model AR = 8.9 and compares the UMR program with NASA data.

The drag for the two aircraft was estimated by using the component build-up method. The drag coefficient of each component was totaled and increased by a factor of 10 percent to account for interference effects as suggested by Roskam[19].

The drag coefficient for the non-lifting components, which influenced the fuselage, nacelles, and vertical tail, was estimated from graphs and equations for turbulent flow about streamlined bodies from Roskam[19], Hoerner[20], and Crawford[21]. The drag coefficient of the lifting surfaces were predicted by the momentum integral boundary layer program and the vortex lattice program as previously described. For each cruise lift coefficient investigated, the two-dimensional drag at the proper Reynolds number and the induced drag at the desired aspect ratio and taper ratio were added to get a total wing drag coefficient. To account for wing interference, a factor of 10 percent of the zero-lift drag coefficient for the two airfoils considered was added to the total wing drag coefficient.

With the basic aircraft sized, drag coefficients and weights estimated, the reduction of configuration drag was completed by optimizing the wing for minimum cruise drag. This included an investigation of taper ratio, winglets, aspect ratio between 6 and 12, and altitude between 9144-12192 m (30-40,000 ft) and staying within the limit of wing loading of 1197-2873 N/m^2 (20 to 60 lb/ft^2). The cruise weight consisted of the aircraft field length requirements. The cruise weight consisted of the aircraft with a full payload plus 20 percent reserve fuel and half the available fuel above reserve.

The wings of the baseline aircraft were designed to utilize winglets to reduce the induced drag. The magnitude of the induced drag reduction was determined by a computer trade-off study which also found the optimum wing taper ratio, λ, at a wing of aspect ratio 12 with taper ratio between 0.2 and 1.0,

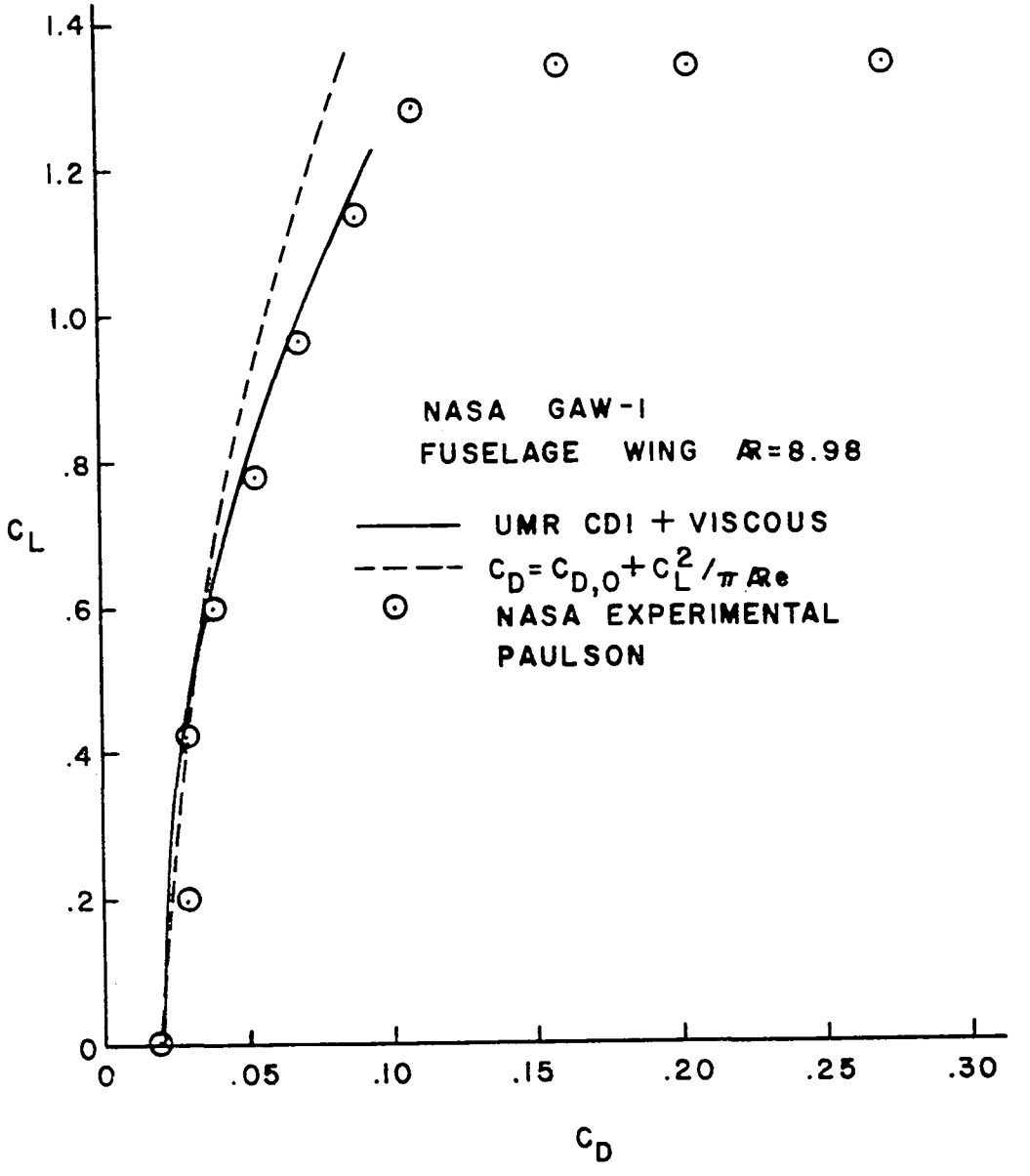

Figure 11. Vortex Lattice Program Comparison.

using the NARUVLE vortex lattice program to compute the induced drag were calculated for the various configurations. The optimum configuration agreed with Whitcomb[22] in terms of dihedral and incidence, although the magnitude of the predicted drag reduction was less. Because of the high degree of correlation between the current study and the NASA study, the standard NASA winglet design of Whitcomb[22] was used. To be conservative, however, the drag reduction value obtained from NARUVLE was used instead of the value indicated by Whitcomb[22]. These results indicate that $\lambda = 0.6$ produces the greatest reduction in induced drag, ΔD_i, below $C_L = 0.44$ and $\lambda = 0.8$ produces the greatest reduction above $C_L = 0.44$. Since it was anticipated that the cruise lift coefficients would be 0.4 or higher, $\lambda = 0.8$ was selected over $\lambda = 0.6$. The induced drag values of the UMR program were modified to account for the effects of adding winglets using the results of the NARUVLE winglet study, giving a 15 percent reduction of the wing induced drag.

The optimization of wing area and altitude for minimum cruise drag was accomplished by the use of a computer program which computed a wing weight for each wing area in the desired range and then found the total aircraft weight, Wt, assuming constant engine weight. This allowed a corresponding lift coefficient to be calculated. At this lift coefficient, the program searched through two- and three-dimensional drag polars to find the two- and three-dimensional drag coefficient for the specific conditions of Reynolds number (altitude) and aspect ratio. The drag of the non-lifting components was computed and added to the wing drag. Minimization of this final drag was the criterion by which the program selected the optimum wing area, aspect ratio, and altitude.

Figure 12 shows a sample of the results of the optimization program for the six-place aircraft configured with the MS(1)-0313 airfoil section and aspect ratio of 8 and 12. Over a wing area range of 6.9 to 27.6 m^2 (75 to 300 ft^2), the minimum cruise drag was obtained at an area of 13.9 m^2 (151.6 ft^2) for the

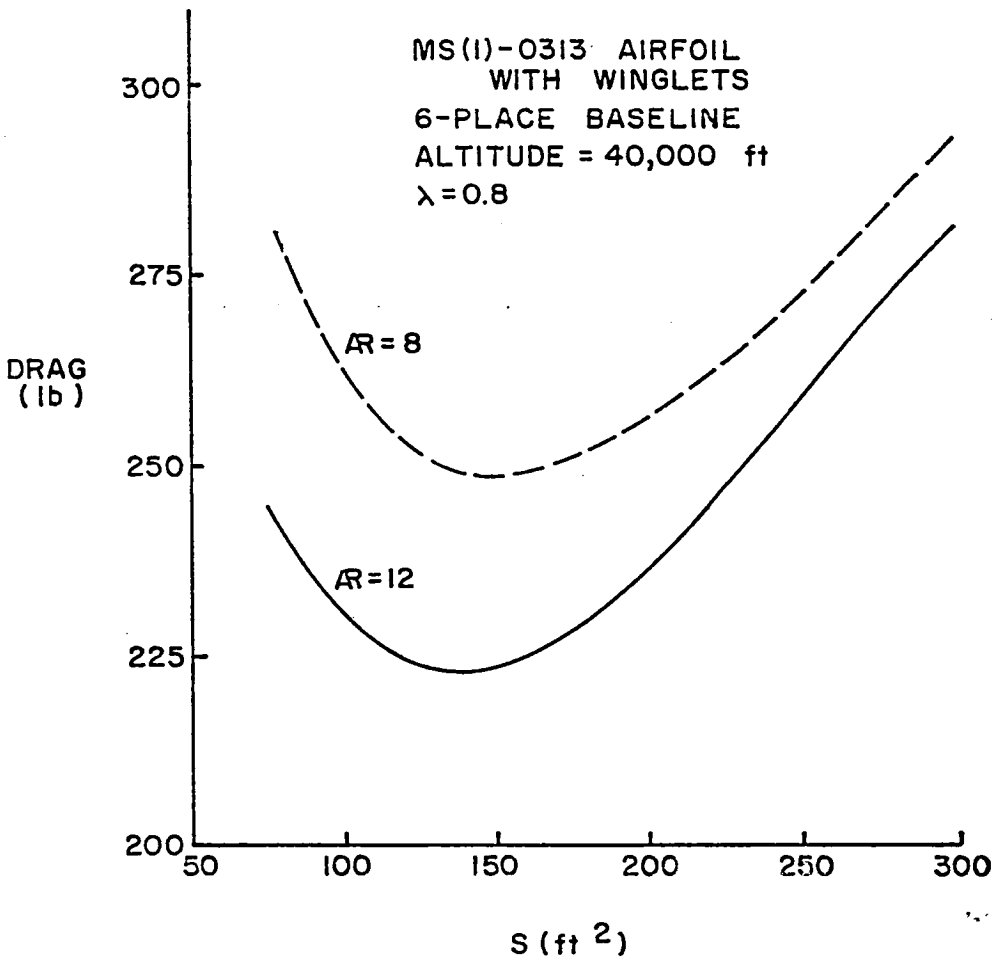

Figure 12. Six-Place Baseline Aircraft Optimization Results.

wing with AR = 8 and 12.7 m^2 (138.6 ft^2) for the wing with AR = 12. The figure also indicates the significant drag reduction, about 10 percent, achieved by increasing the aspect ratio from 8 to 12.

Based on the results obtained by the optimization program, an altitude of 12,195 m (40,000 ft) was selected as being the best cruise altitude. Since the aircraft were arbitrarily limited to an aspect ratio of 12 or less, an aspect ratio of 12 was chosen for its low minimum drag values.

Using the techniques of Roskam[23,24] a static stability program was generated which aided in determining the wing location, horizontal and vertical tail sizes, and static stability derivatives. Accounting for the aerodynamic center, a.c., shift due to the body and all possible loading conditions at cruise flight, longitudinal, lateral, and directional stability was obtained which is comparable to that found on typical light and business aircraft. No dynamic analysis was performed.

The trim performance for each aircraft was completed by obtaining a zero pitching moment at cruise flight conditions. This was accomplished by finding the required tail lift coefficient for trim flight and the two- and three-dimensional drag associated with it. The drag was determined by the use of the momentum integral boundary layer program and the vortex lattice program as previously described. The additional trim drag was calculated, and the untrimmed data obtained from the optimization program was modified accordingly.

Canard Results

The six- and twelve-place canard aircraft were designed to meet the same requirements as outlined for the baseline aircraft. Each used the same fuselage, vertical tail, and engines, and both aircraft were optimized at an altitude of 12,195 m (40,000 ft). The canard and wing have a taper ratio equal to 0.8, while only the wing utilized weights. Since the canard is forward of the c.g.,

winglets were not used on the canard, thus maintaining the same directional stability as the baseline without increasing the vertical tail size. The aspect ratio was defined individually for both lifting surfaces as the square of the individual span divided by the reference area of the individual lifting surface. The component weights of the canard aircraft are identical to the baseline aircraft except for the lifting surface weights. Each lifting surface weight was estimated as described for the baseline aircraft, but based on the maximum percentage load it carried. There were two versions of the six- and twelve-place canard aircraft, one with the MS(1)-0313 airfoil for both the canard and wing, while the other version utilized the NL(S)-0715F airfoil on both lifting surfaces.

The terms associated with canard configurations are gap, G, stagger, S, and decalage, D. Gap is the vertical distance between the canard and wing and is always considered positive. Stagger is the horizontal distance between the canard and the wing with positive stagger occurring when the canard is above the wing. Decalage is the relative angle of attack between the canard and wing, positive when the canard is at a higher angle of attack than the wing. Both stagger and gap are measured from mid-chord to mid-chord and non-dimensionalized with respect to the average chord length of the wing and canard. The dividing line between canard and tandem wing configurations is somewhat arbitrary and not really important here. For this investigation, it is assumed that a canard configuration is one in which the forward surface area is equal to or less than the rear surface area. Also, any configuration with samll stagger, less than two average chord lengths, is considered to be a dual wing configuration.

The canard aircraft designs maximized the results of the aerodynamic trade-off analysis completed by Keith[25], but to obtain "flyable" aircraft with minimum cruise drag, consideration was given to certain design constraints as:

canard and wing as related to gap and stagger; stability and control which determined the possible locations of the wing and canard; trim, stall, and take-off rotation which determined the decalage angle and wing to canard area ratio. The results of Keith's study indicate the following desired features for successful canard designs:

1. Aspect ratio of wing and canard should be as large as possible.
2. The stagger between the wing and canard should be as large as possible.
3. The decalage angle should be kept as small as possible to avoid high two dimensional drag values.
4. The gap between the canard and wing should be as large as possible.

As a result of the above desired features, the gap between the canard and the wing was chosen such that the canard and wing were at the top and bottom of the fuselage. This maximized interior fuselage usage while transferring lifting surface loads to the fuselage with minimal added weight. In order to have the largest possible stagger the canard needed to be as forward as possible, and when visibility is considered a positive stagger, canard above the wing chosen. As a side benefit negative stagger systems have earlier boundary layer separation than positive stagger systems.

Since the altitude and wing taper ratio were optimized in the baseline study, only the total wing area was optimized and selected to obtain minimum cruise drag for the canard aircraft. Figures 13 and 14 show the weighted drag coefficient ($C_D \times S$) as a function of the total wing area considered for various wing-to-canard area ratios. These figures present the breakdown of the two dimensional and induced drag coefficient as well as the total drag coefficient for the six-place canard aircraft with the MS(1)-0313 airfoil and NL(S)-0715F airfoil, respectively. Figure 13 shows that the MS1 two dimensional drag increases at almost the same rate as the three dimensional induced drag decreases, with

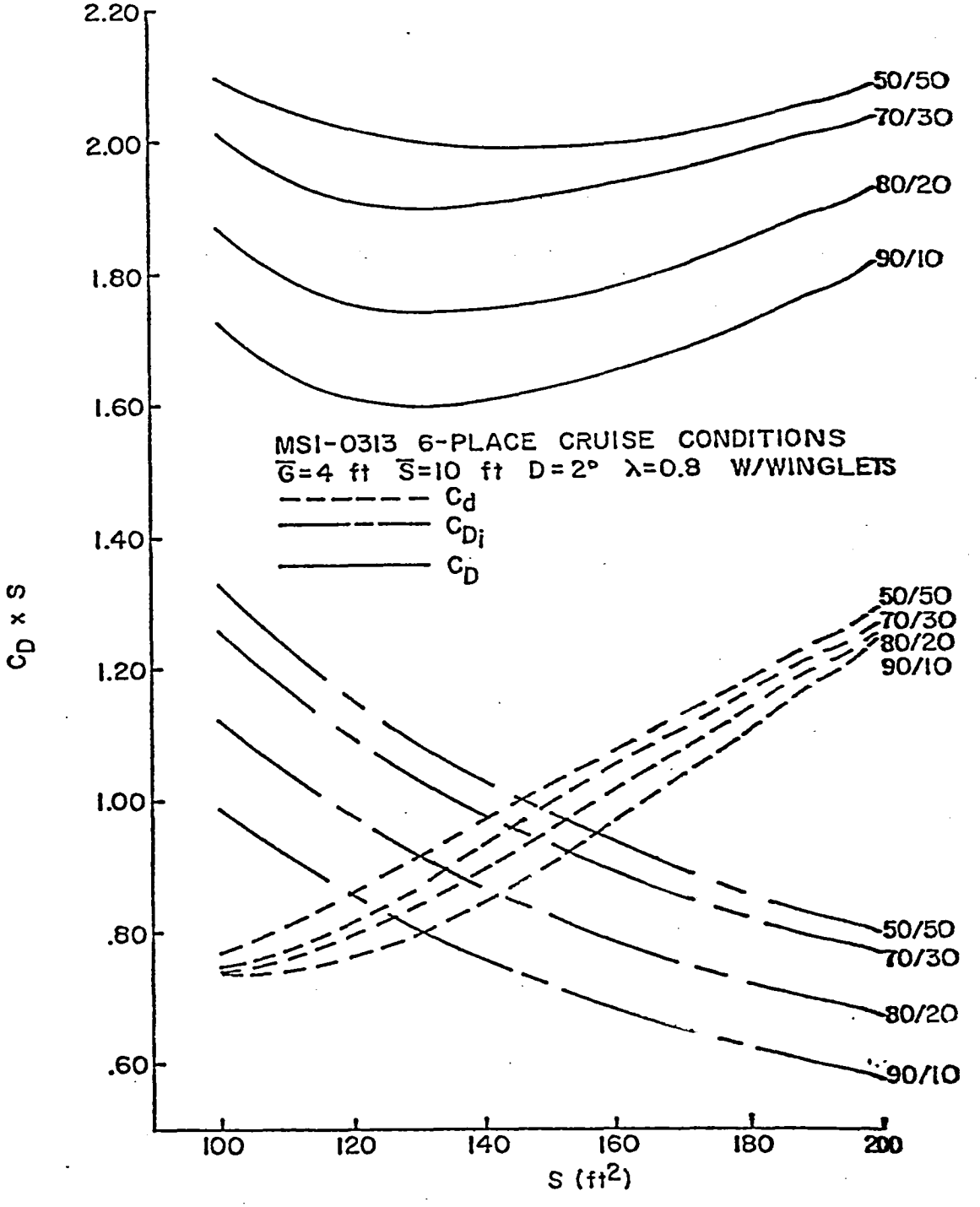

Figure 13. Weighted Drag Coefficient for the Six-Place MS(1)-0313 Canard Aircraft.

increasing wing area. The minimum total drag occurs close to the intersection of the two drag components, at which point the two are equal, i.e., a total wing area between 11.9 m^2 (130 ft^2) and 13.8 m^2 (150 ft^2) for all wing-to-canard area ratios. However, the NL(S)-0715F two dimensional drag does not increase as rapidly as does the MS(1)-0313 two dimensional drag for increasing wing area, because of the large and shallow two dimensional drag bucket of the NLS airfoil section. This also results in a large shallow drag range for the NLS version of the six-place canard aircraft as illustrated in Figure 14. But since the induced drag decreases more rapidly than the two dimensional drag increases, the minimum drag for the NLS version occurs at a wing area equal to 18.4 m^2 (200 ft^2), a much higher total wing area than for the MS1 version. Similar trends occur for the twelve-place canard aircraft with total wing area between 18.4 m^2 (200 ft^2) and 41.3 m^2 (450 ft^2). The minimum total weighted drag coefficient for the MS1 version of the twelve-place occurs at wing areas between 24.8 m^2 (270 ft^2) and 28.5 m^2 (310 ft^2) for the various wing-to-canard area ratios, the locations where the two- and three-dimensional drag terms are almost equal.

Applying the trim analysis results in Figure 15. Trim did not produce any additional drag. This figure shows the trim regions for canard configurations with wing-to-canard area ratios of 50/50 and 80/20, and also the trim region for a comparable conventional tail-aft configuration. These results were obtained from the unoptimized baseline and canard designs for the six-place aircraft with the MS(1)-0313 airfoil having equal reference areas of 9.29 m^2 (100 ft^2). The canard designs include a region of trim decalage from -4° to 4°, while the tail aft configuration includes a trim region of horizontal tail lift coefficient $-0.3 < C_{L_H} < 0.3$. This figure shows how the off-optimum load penalizes the conventional tail aft as compared to the canard configurations. The minimum L/D for trim of the canard design is much higher than the tail-aft design minimum L/D for trim.

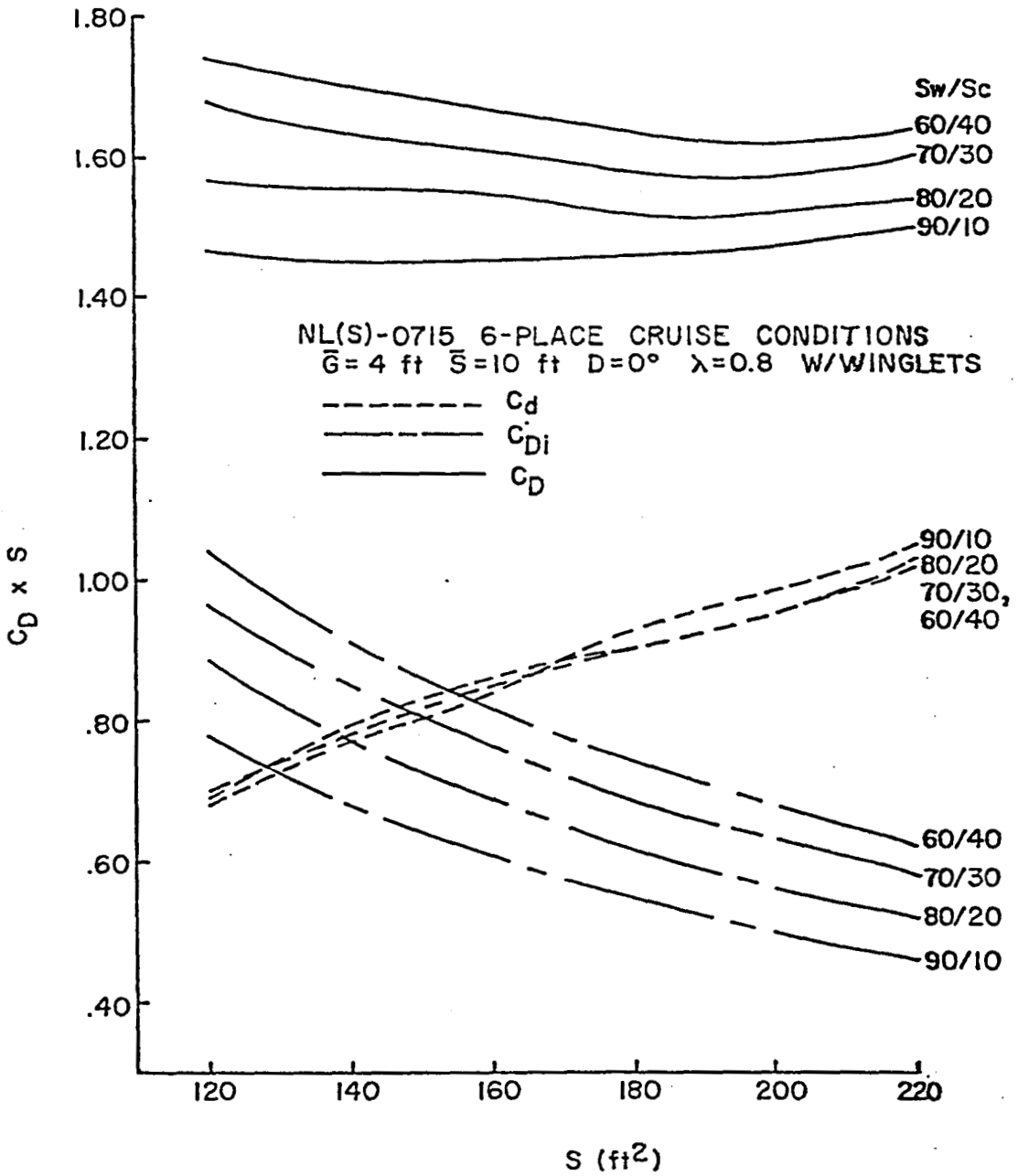

Figure 14. Weighted Drag Coefficient for the Six-Place NL(S)-0715F Canard Aircraft.

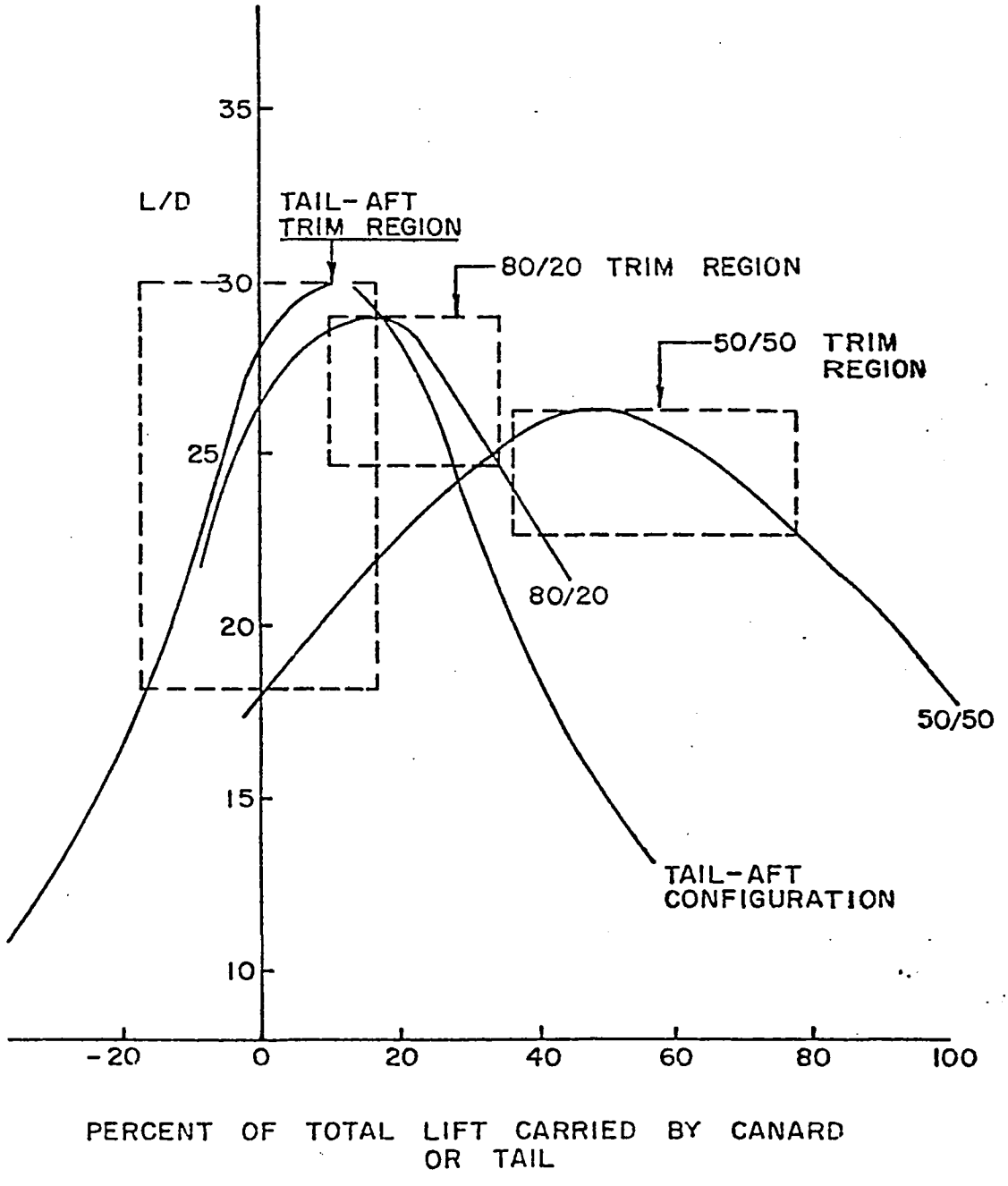

Figure 15. Trim Comparison between Canard and Tail-Aft Configurations.

The trim decalage angle is the relative angle of attack between the canard and wing which produces a zero pitching moment, $C_M = 0$, for the aircraft at cruise level flight. Figure 16 shows C_M as a function of decalage angle for the different wing-to-canard area ratios for the six-place canard aircraft. The pitching moment is very sensitive with decalage angle for wing-to-canard area ratios of 70/30 or less. The high wing to canard ratios require a large trim decalage angle which raises the total drag. These same trends exist for other total lifting areas. Static longitudinal stability requires that $(W/S)_c C_{L_{\alpha_c}} > (W/S)_w/C_{L_{\alpha_w}}$ [26]. Since the same airfoil was used for the canard and the wing and with the stagger relatively large, the surfaces are essentially uncoupled such that $C_{L_{\alpha_c}} \simeq C_{L_{\alpha_w}}$. Thus $(W/S)_c > (W/S)_w$ and hence the high decalage requirement as S_w/S_c approaches 90/10. Figure 17 shows the trim drag for the MS(1)-0313 six-place canard configuration. The trim drag for the six-place NLS-0715F canard configuration is shown in Figure 18.

The final configurations chosen for the canard aircraft have wing areas that yield minimum trim drag at an area ratio equal to 70/30 for the MS1 airfoil and 80/20 for the NLS airfoil. Since the trim drag for all area ratios is almost equal, it was desirable to select the highest possible area ratio, without being penalized severely for drag, so that minimum lift would be lost in a stall situation. Since the canard is at a greater incidence angle than the wing, it is anticipated that the canard would always stall first, and with minimum area chosen for the canard, less total lift would be lost. Also for the 80/20 area ratio, all the fuel could be placed in the wing without any fuselage fuel cell. The drag for the 50/50 area ratio was less, but the location of the wing would be too far aft and could not be feasibly located on the fuselage tailcone.

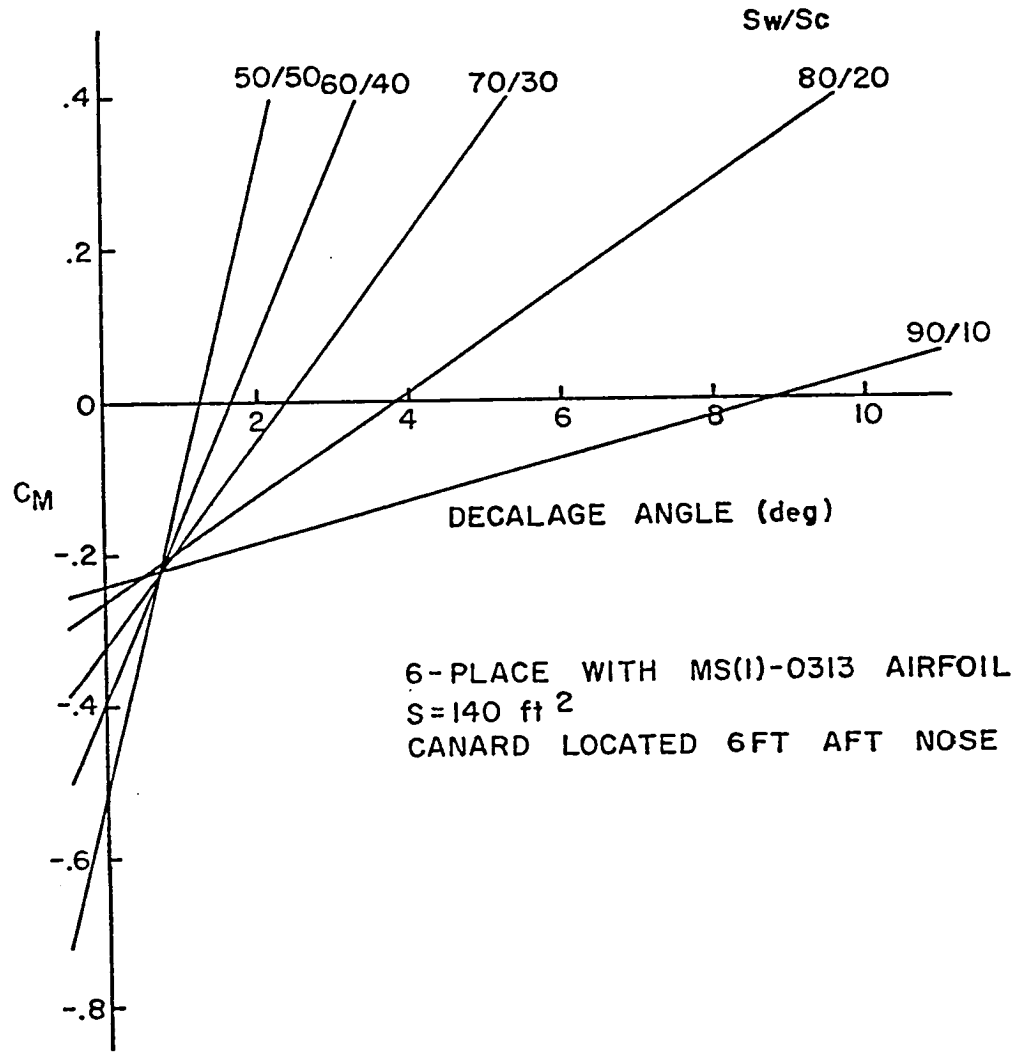

Figure 16. Pitching Moment Coefficients for the Six-Place Canard Aircraft.

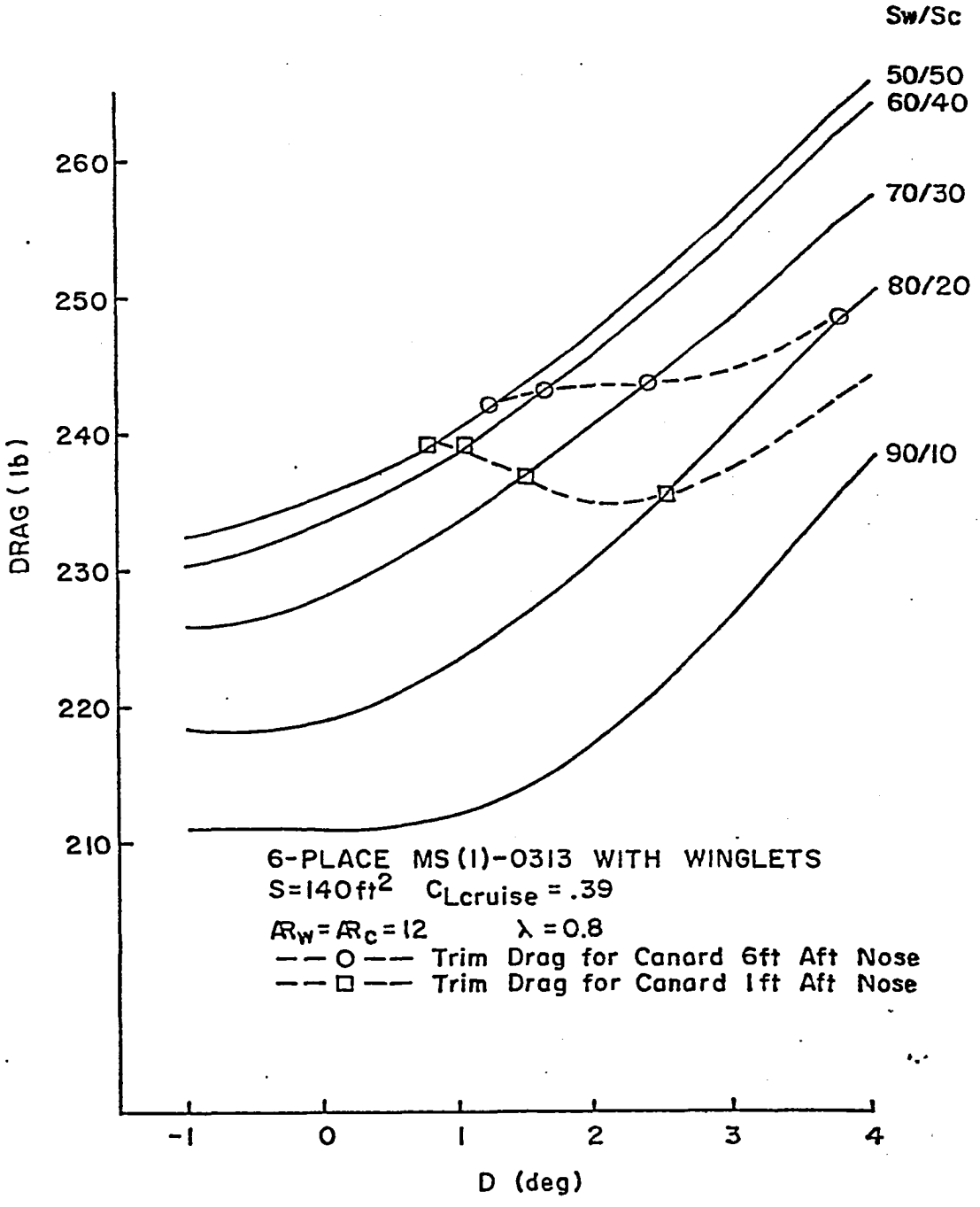

Figure 17. Sample Trim Drag Optimization Curves for the Six-Place MS(1)-0313 Canard Aircraft.

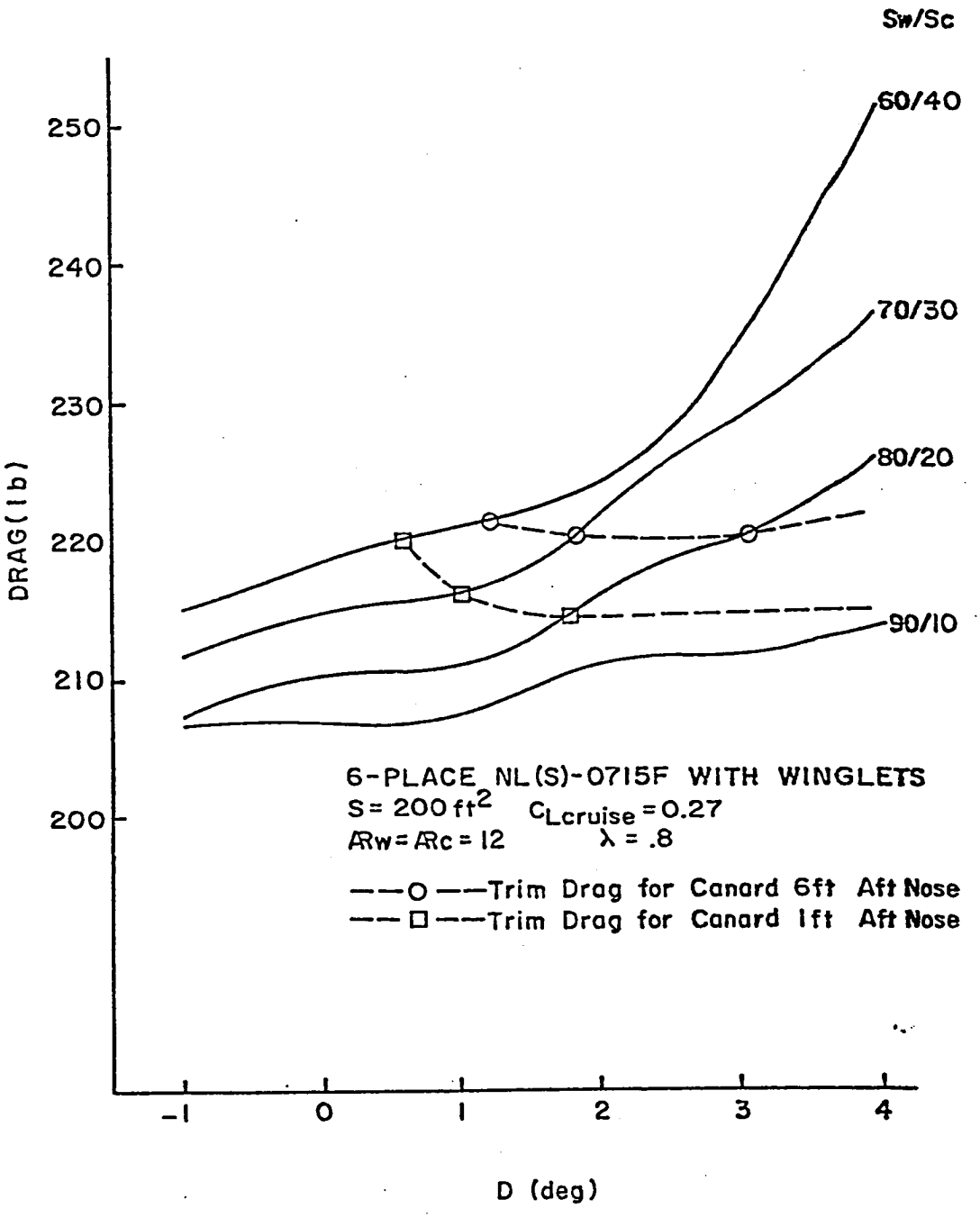

Figure 18. Sample Trim Drag Optimization Curves for the Six-Place NL(S)-0715F Canard Aircraft.

It should be mentioned that although the canard does have a slight drag and hence range penalty with respect to the baseline, the absence of stall problems and hence spin more than offsets these range penalties. Also mixing the airfoil sections of the canard and the wing should provide better performance for the canard configuration.

Dual Wing Results

Several investigators have shown that closely coupled dual airfoil systems can have superior two dimensional aerodynamic performance with proper stagger, gap, and decalage[26,27,28,29,30,31]. Analytical procedures developed in 1934 by Prandtl and Tietjens[32] determined that some dual wing configurations would have lower induced drag than an equivalent single wing.

Vortex panel methods as described earlier were used for the two dimensional predictions along with momentum integral techniques and the Squire-Young formula for drag coefficient.

Initial investigation of the performance of various dual wing configurations covered a wide range of staggers to confirm the observations of previous dual wing research[10,30,31]. These investigations showed that negative stagger caused higher drag and much earlier separation. This is shown in figure 19. The negative stagger runs (curves E through H) invariably exhibited flow separation at relatively low lift coefficients, while the positive stagger, negative decalage cases (curves B through D) delayed the separation point to lift coefficients of 1.5 or greater. The positive stagger, positive decalage run (curve A) separated at a lift coefficient of less than 0.8 and produced an excessive amount of drag. Likewise, the negative stagger configurations created large amounts of drag in relation to the positive stagger, negative decalage cases. All of these findings supported the conclusions reached by Norton[26], Nenadovitch[30], and Olson and Selberg[31], who determined that both the negative

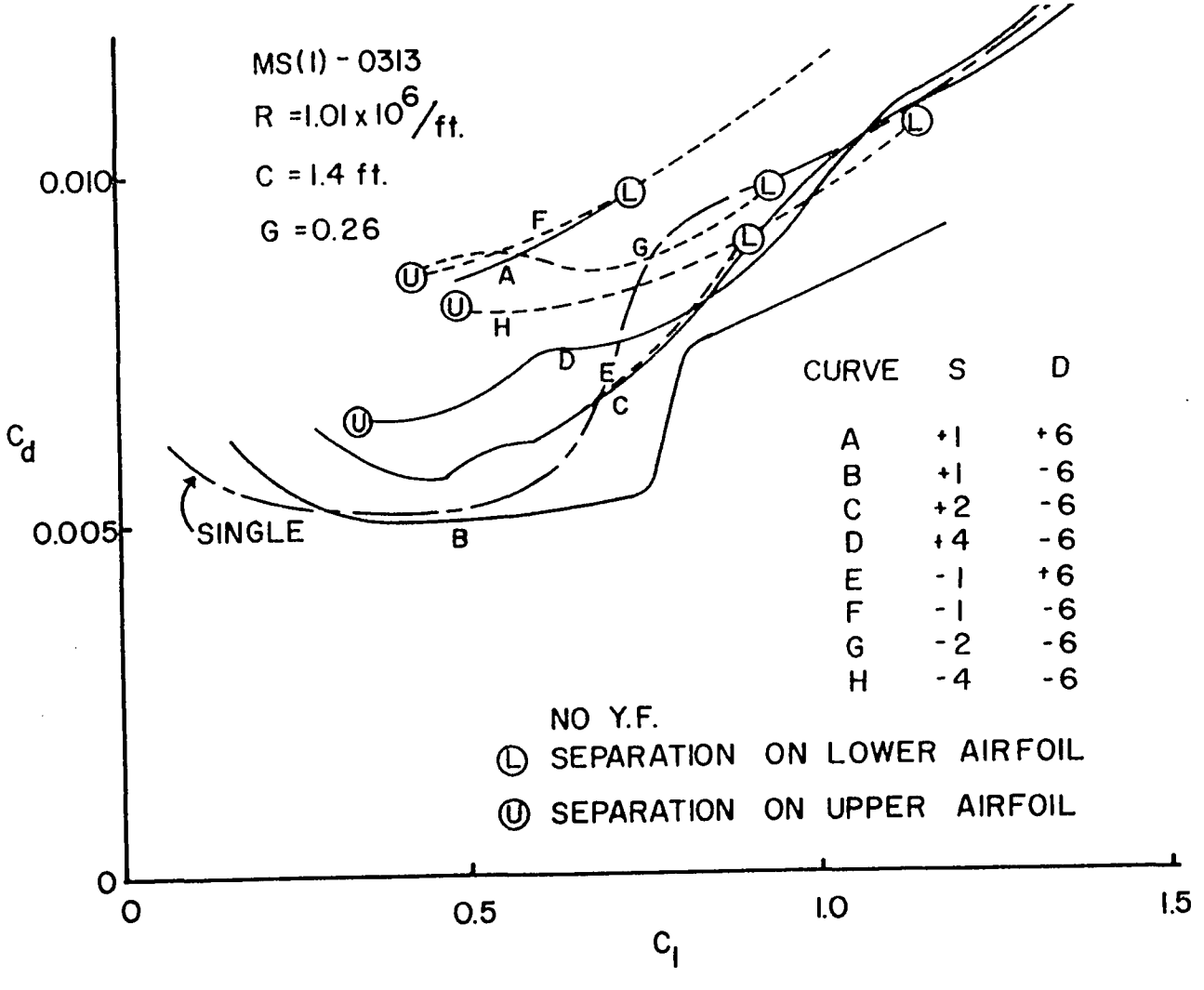

Figure 19. Dual Airfoil Two Dimensional Drag Polars.

stagger and the positive decalage configurations performed poorly compared with the positive stagger, negative decalage condition. The NL(S)-0715F airfoil displayed similar behavior. Due to the above results all optimization studies were directed in the region of positive stagger and negative decalage. The optimization study investigated changes in positive stagger, negative decalage angle, and gap. Details of this optimization are found in (33), (34). The optimum airfoil placement from two dimensional considerations for airfoils of equal chords is a stagger of 1.0, a gap of 0.26, and a decalage angle of -6 degrees. Figure 20 presents the C_ℓ/C_d results of this optimum airfoil placement showing a significant improvement in liftover drag at the higher lift coefficients. Figure 21 shows the pressure distribution for two airfoil sections at a stagger of 1.0, a gap of 0.26, and a decalage of -6 degrees. For the case, the lower wing at a geometric angle of attack, α, of 1 degree obtained a lift coefficient, C_l, of 0.439, comparable to that of a single wing at a -1 degree angle of attack. The upper wing produced a lift coefficient of 0.559 at a geometric angle of attack of -5 degrees, which is approximately equal to the lift on a single wing at a 0 degree angle of attack. Thus, the upper and lower wings receive a +5 degree and a -2 degree induced angle of attack, respectively, indicating that the flow about each wing is significantly affected by the presence of the other wing. Figure 21 also illustrates the reduced leading edge pressure peak and the reduced adverse pressure gradient experienced by the dual wings, both of which inhibit boundary layer separation.

Upper surface transition location for a stagger of 1.0, a gap of 0.26, and a decalage of -6 degrees is shown in Figure 22. The transition points for both the dual wing and the single wing configurations were at about 60% and 10% chord for low and high lift coefficients, respectively. However, the shift from transition at 60% chord to transition at 10% chord occurred at list coefficients of 0.6 to 0.8 for the single wing, as opposed to 0.9 to 1.1

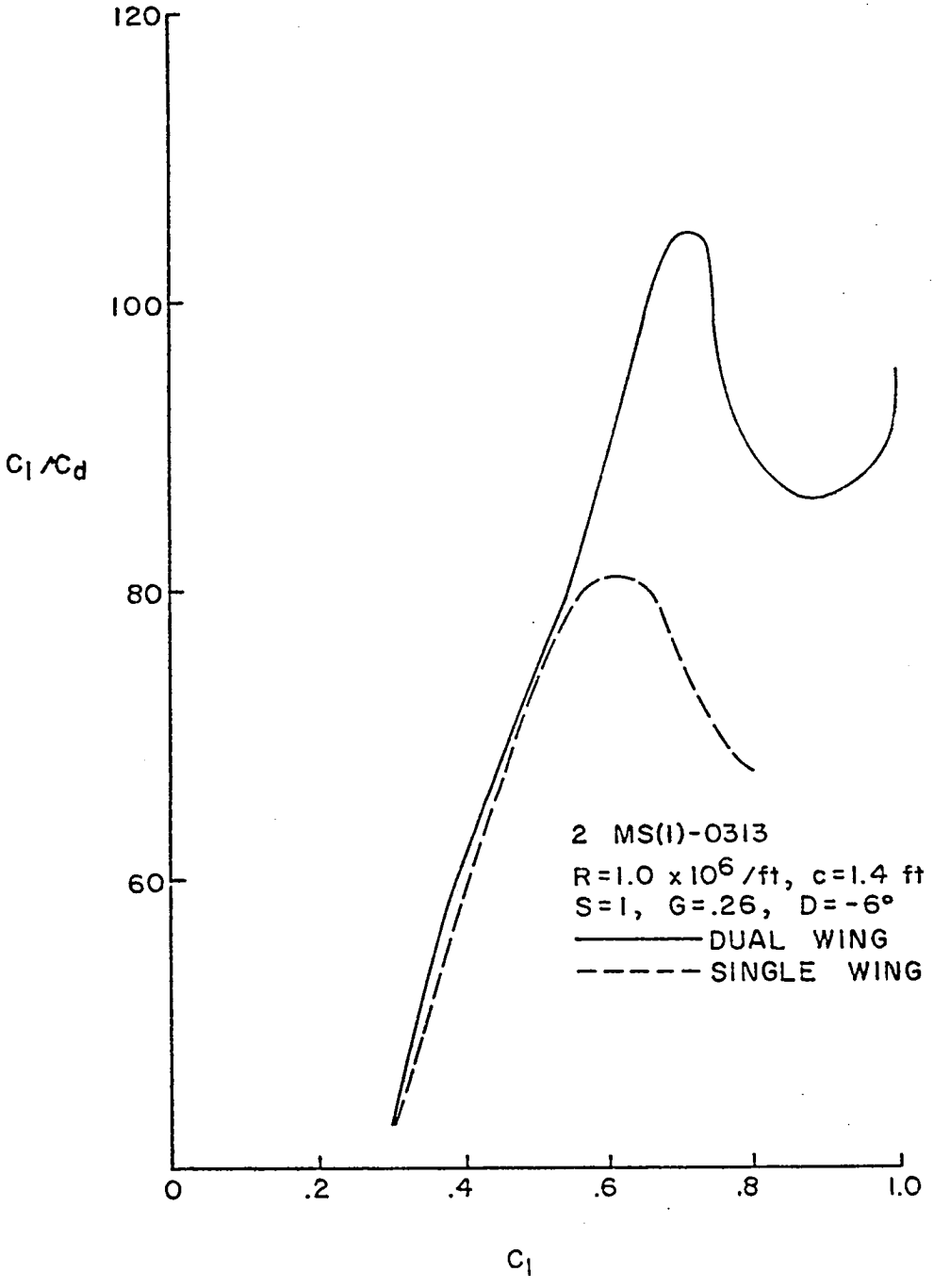

Figure 20. Dual Airfoil Optimum Results for MS(1)-0313.

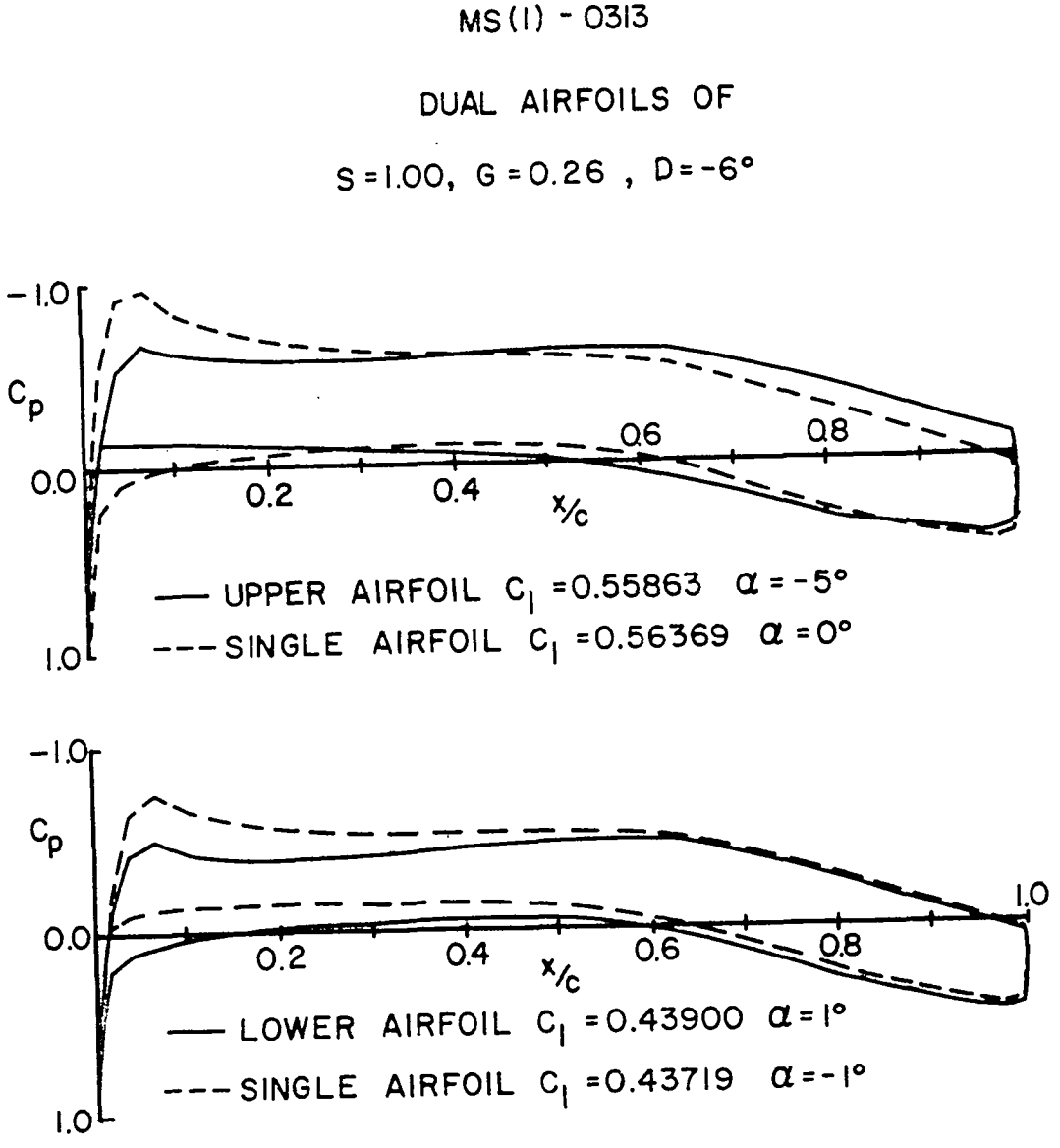

Figure 21. Dual and Single Airfoil Pressure Distributions.

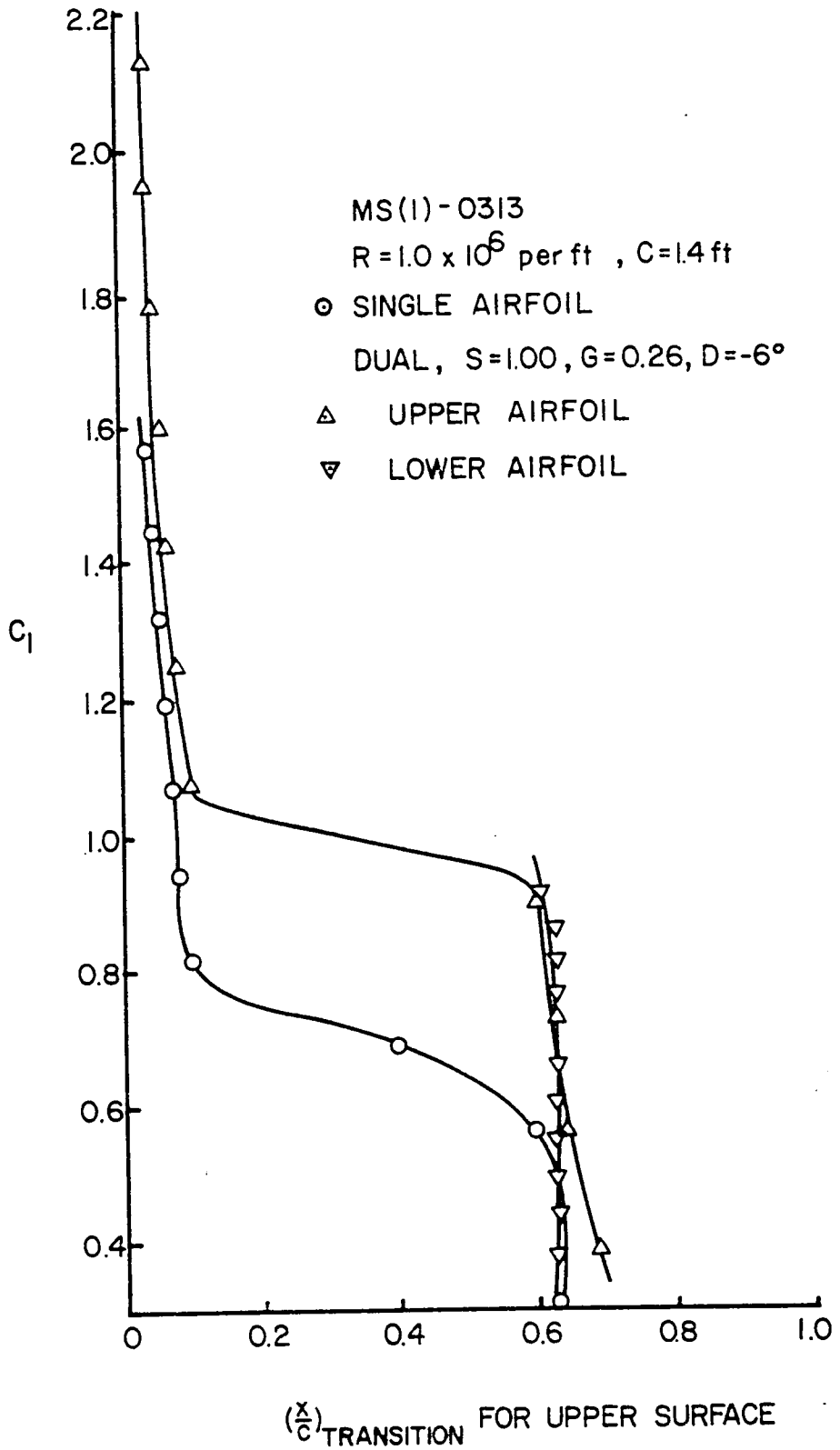

Figure 22. Boundary Layer Transition Location for MS(1)-0313.

for the dual wing configuration. The essence of this behavior is that the dual wing benefits from a considerably longer period of laminar flow between lift coefficients of 0.6 and 1.1 and a corresponding decrease in viscous drag. Similar trends were obtained for the NL(S)-0715F. While the same transition shift occurs that happened for the MS(1)-0313 it occurs at much higher lift coefficients thus reducing its value at normal cruise lift coefficients.

Induced drag comparisons between the various configurations were also conducted, using the three-dimensional UMR vortex lattice program. The results of this study indicated that the difference in induced drag between various closely coupled dual wing configurations was considerably less than the corresponding difference in two-dimensional drag over the range of stagger, gap, and decalage investigated. The study covered wings of aspect ratios 12 and 16. Figure 23 shows a sample of the cases investigated, and illustrates the induced drag advantage of the dual wing over a single wing of equivalent aspect ratio, i.e., a single airfoil with the same span, b, and area, S_{ref}, as the dual wing, and whose chord is equal to the sum of the two dual wing chords. The figure also indicates the significantly lower induced drag of the aspect ratio 16 wing compared to the wing of aspect ratio 12. Since the two dimensional savings were more dominant in the final design, a constant stagger, gap, and decalage with span configuration was chosen, i.e. stagger of 1.0, gap of 0.26, and decalage of -6 degrees.

The results of the optimization program with trim is shown in Figure 24 as a function of area. The cruise lift coefficient for the dual wing is between 0.55 and 0.66 depending on payload. Figure 25 shows the two dimensional savings that occur at the higher lift coefficients for the dual wing configuration. The dual wing in this study was penalized because of having

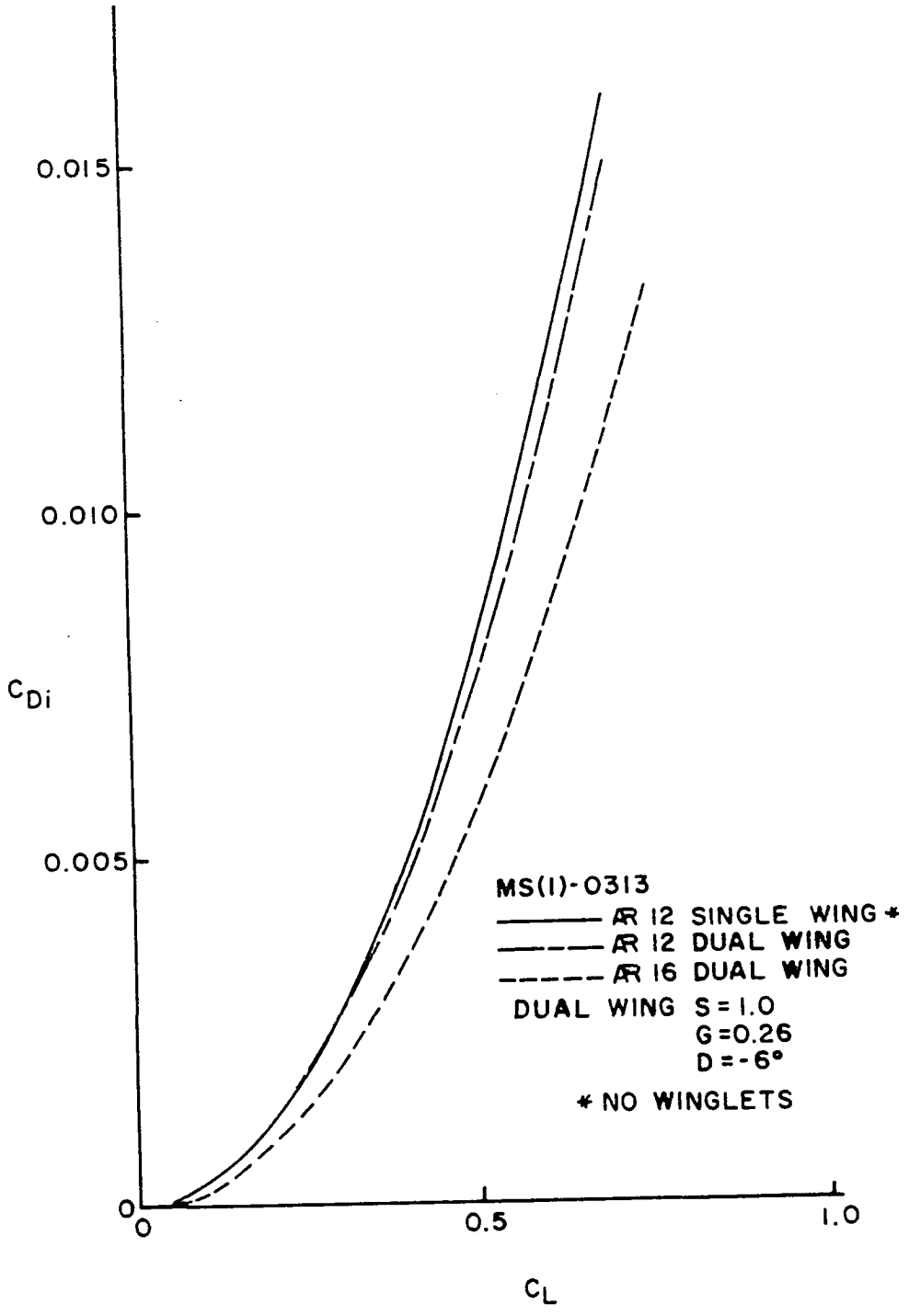

Figure 23. Induced Drag Results for Dual and Single Airfoil Wings.

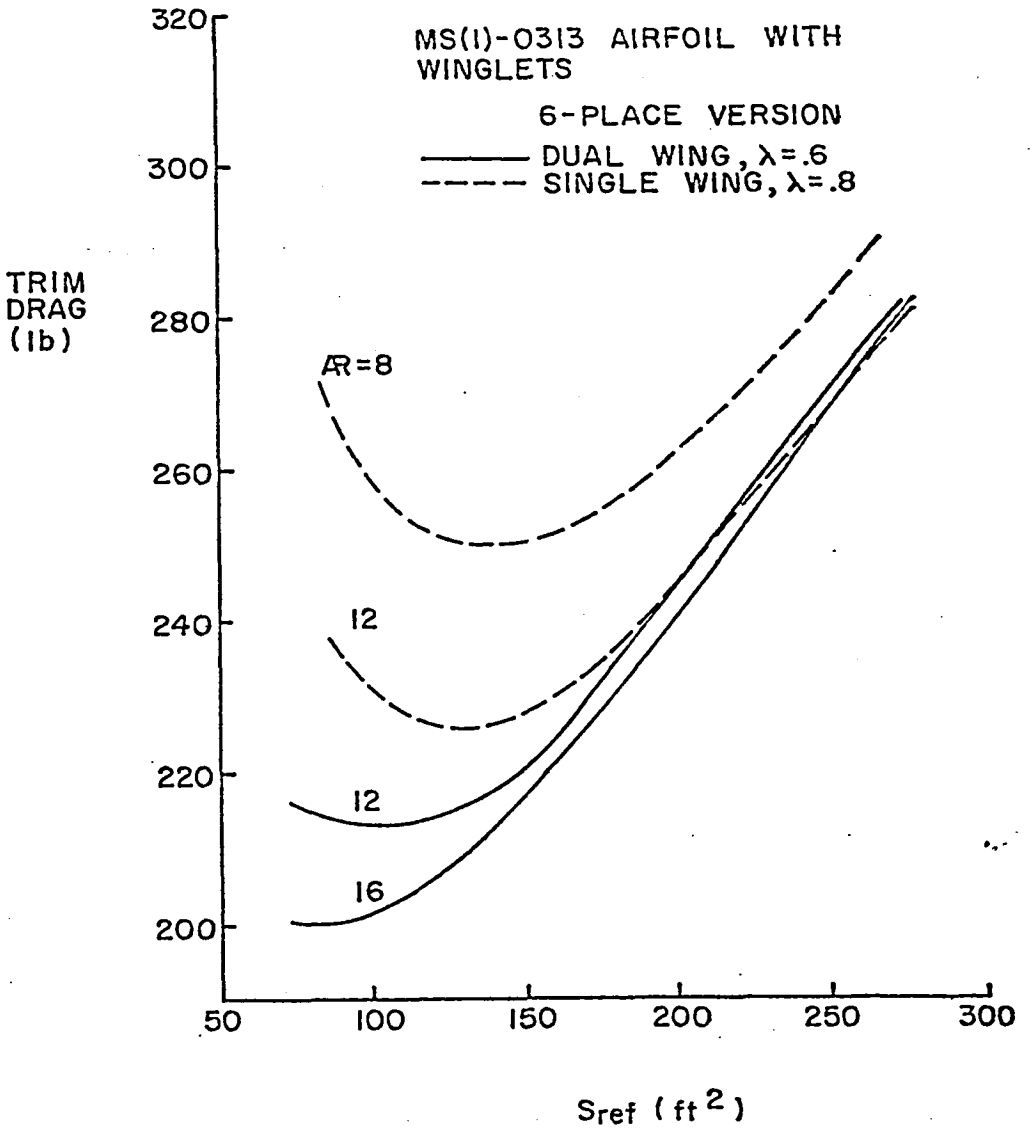

Figure 24. Trim Drag Optimization Results for Dual and Baseline Aircraft.

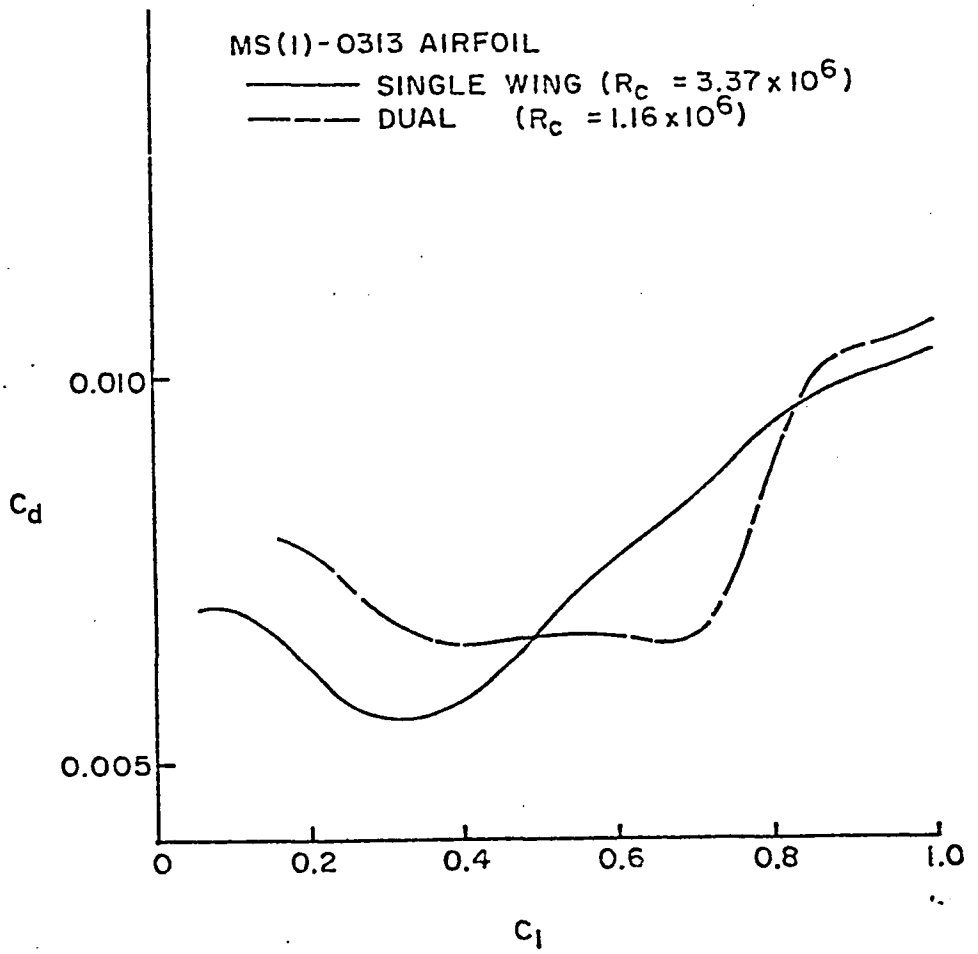

Figure 25. Dual and Single Airfoil Two Dimensional Drag Polars.

to operate with an airfoil that was so much below its design Reynolds number. If the design specifications had been different such that higher Reynolds numbers were required then figure 26 illustrates the two dimensional savings with a stagger of 1.0, a gap of 0.26, and decalage angles of -4, -6, and -8 degrees. For these cases the drag coefficient is below the single, for lift coefficients between 0.1 and 1.0 allowing for decalage area tuning for minimum drag. The dual airfoil results were also penalized because the utilized airfoil sections were not designed to operate in the closely coupled mode.

Swept Forward Swept Rearward Configuration Results

The SFSR configuration utilized the results of the dual wing portion of the study in eliminating negative stagger configurations due to their higher two dimensional drag and early boundary layer separation. Since the SFSR configuration was to be joined at the tip and since the dual airfoil studies already established that a S = 1.0, G = 0.26, and D = -6 degrees resulted in the best aerodynamic behavior, the tip geometry was fixed at these values. Three-dimensional SFSR studies were conducted to investigate stagger and decalage versus span variations. Figure 27 shows induced drag as a function of lift coefficient at various staggers. The induced drag decreases with decreasing stagger, however, since all the longitudinal control is exerted by the wings the minimum S_{root} was chosen while still maintaining sufficient control power in the form of $C_{m_{\delta_E}}$, i.e. a value equal to the baseline designs. This occurred when $S_{root} = 8$. Gap and decalage variations at the tip are shown in Figure 28. A root decalage of 0.0 degrees is superior to a root decalage of -6 degrees thus providing a geometric washout from root to tip. The span variation of lift distribution of the front and rear wings at a $C_L = 0.6$ and a $S_r = 8$ is shown in Figures 29 and 30 as a function of G_r and D_r. Both curves, A and D, are approaching the elliptical

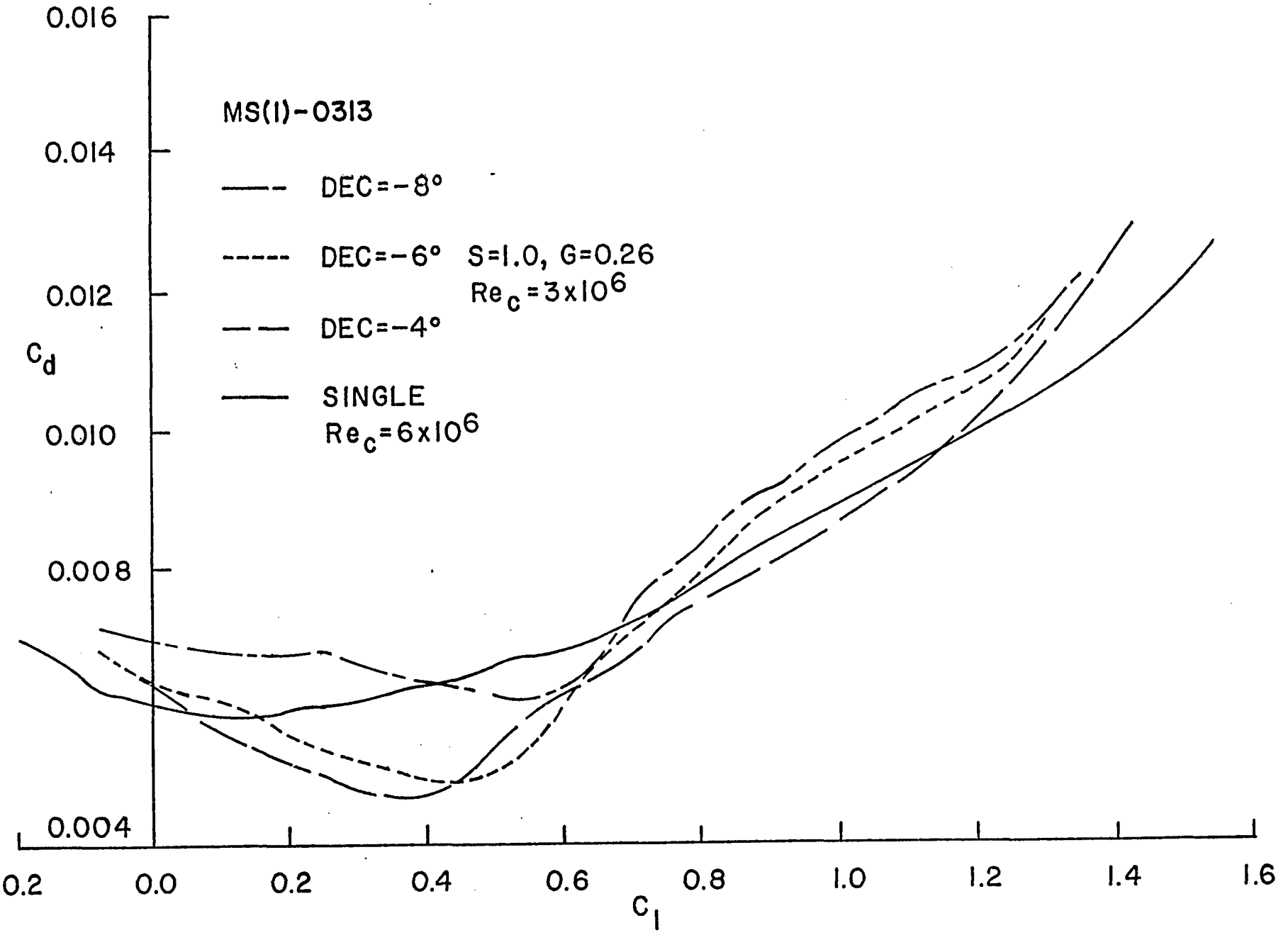

Figure 26. MS(1)-0313 Dual Airfoil Two Dimensional Drag Polars.

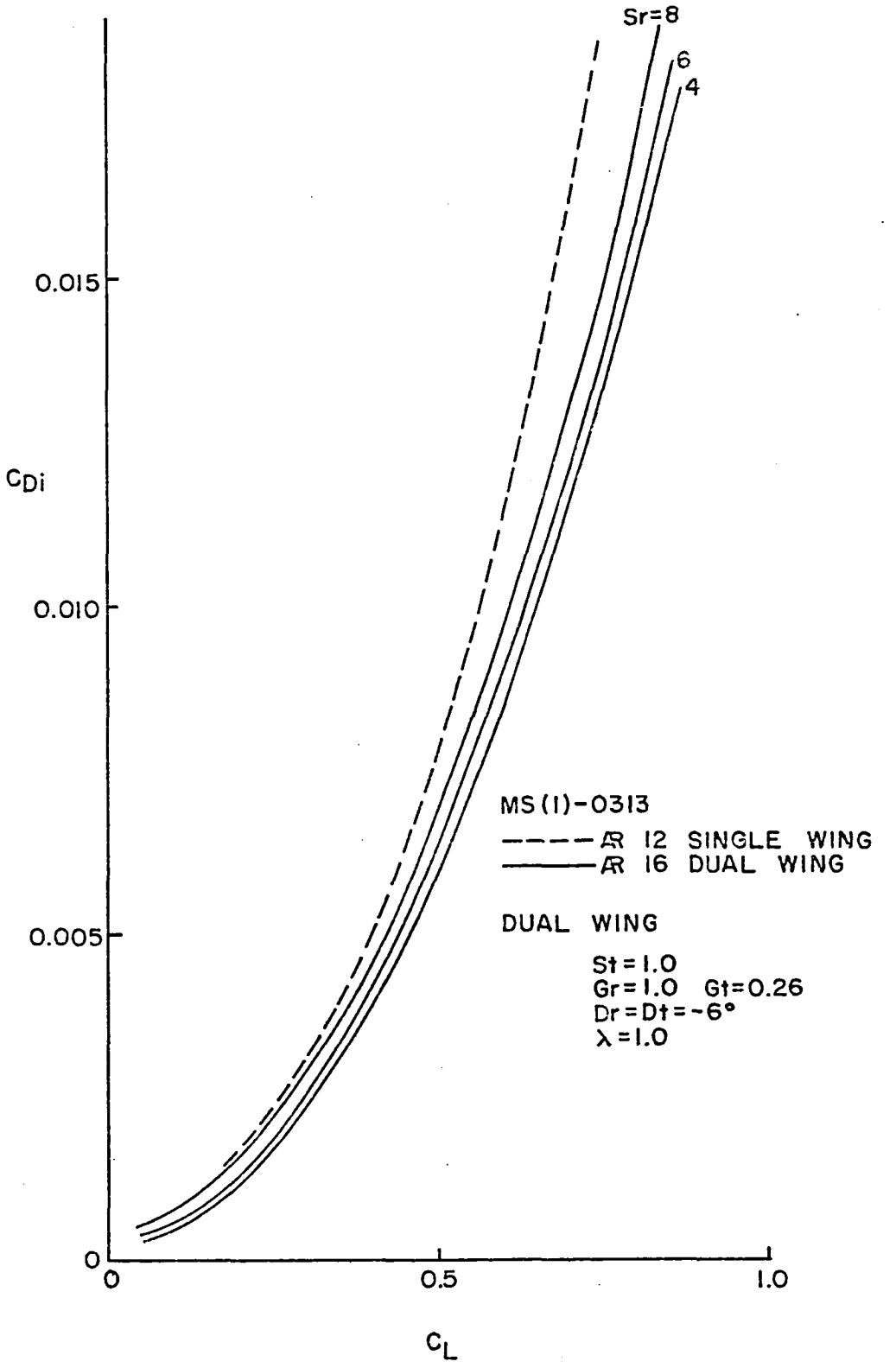

Figure 27. SFSR Configuration Induced Drag Results for Various Staggers.

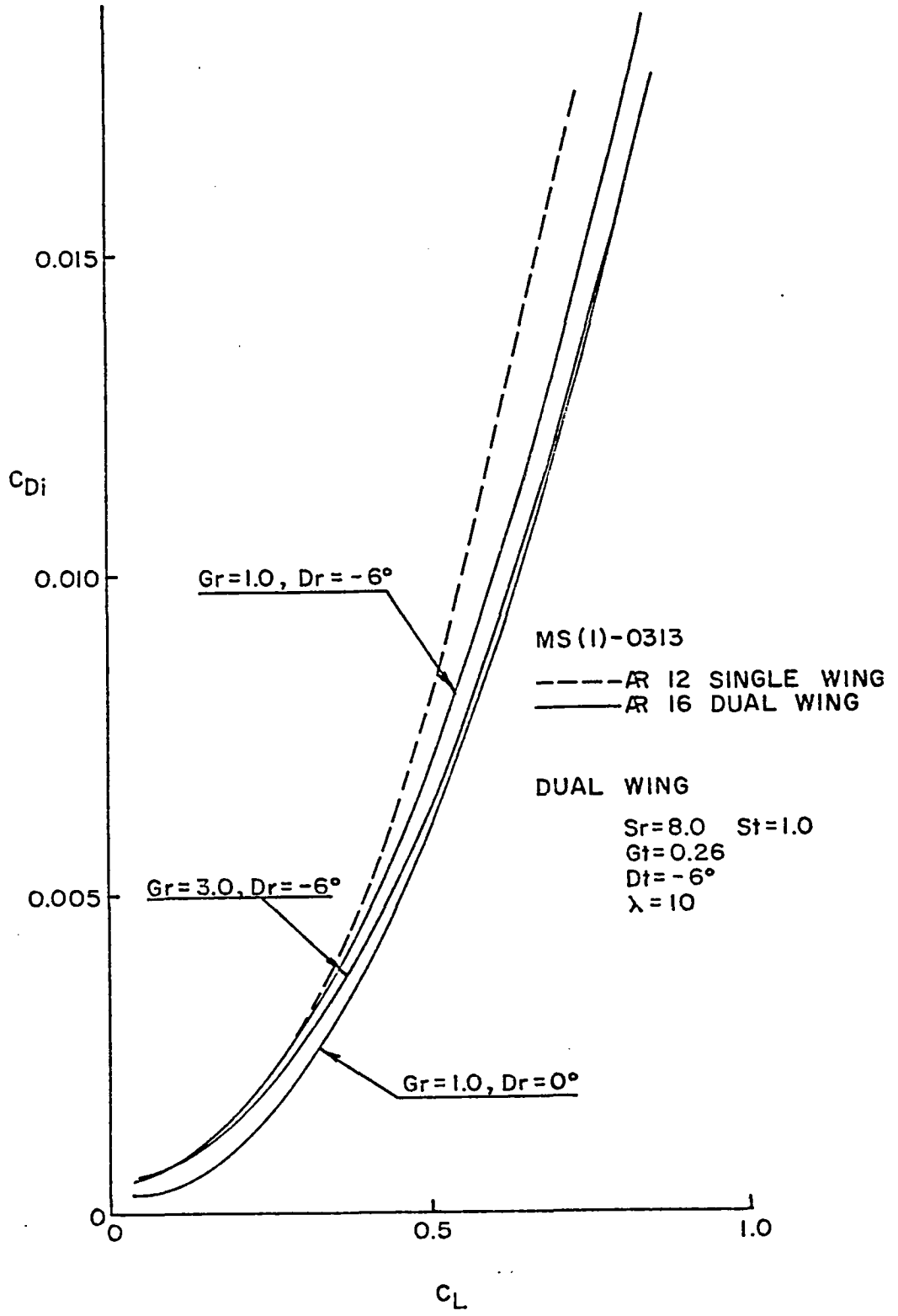

Figure 28. Induced Drag Variations with Gap and Decalage for the SFSR Configuration.

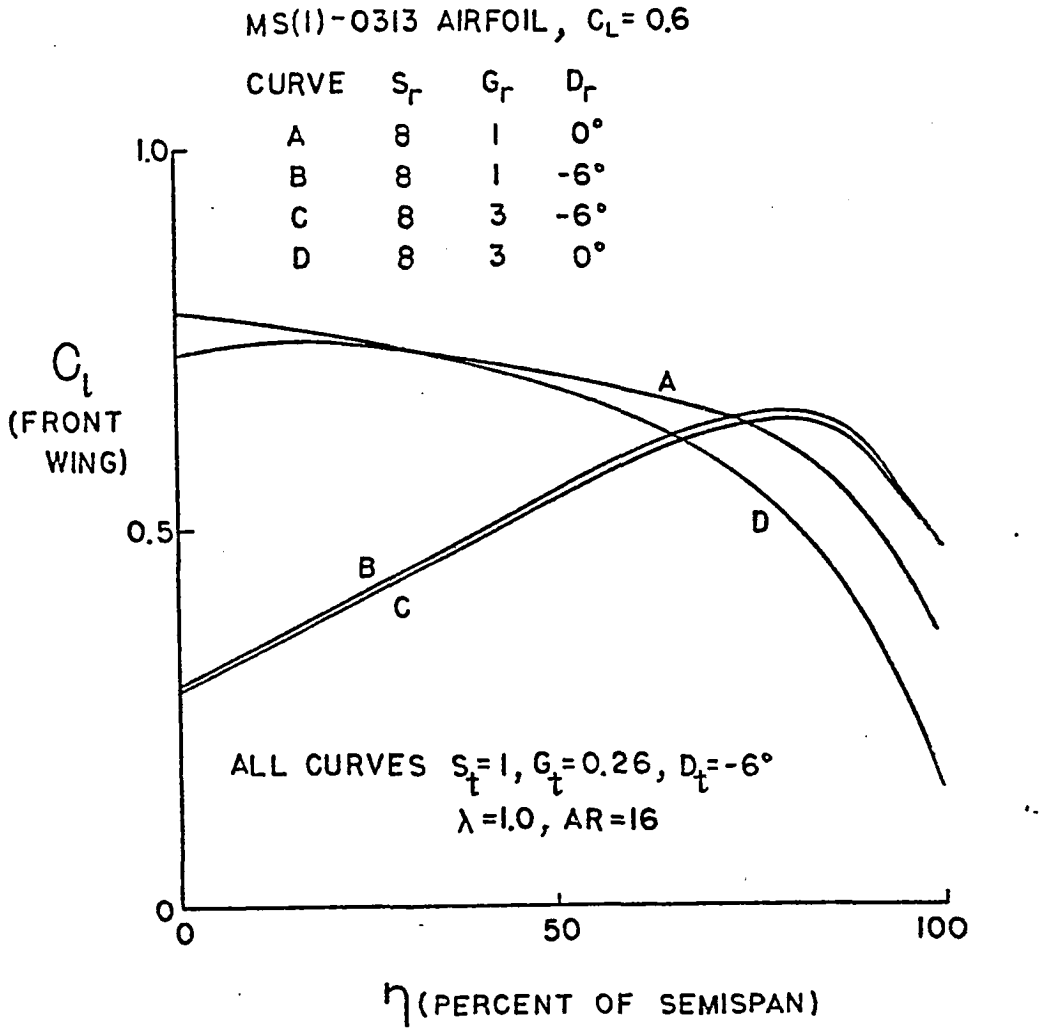

Figure 29. Front Wing Span Lift Distribution for Gap and Decalage Variations.

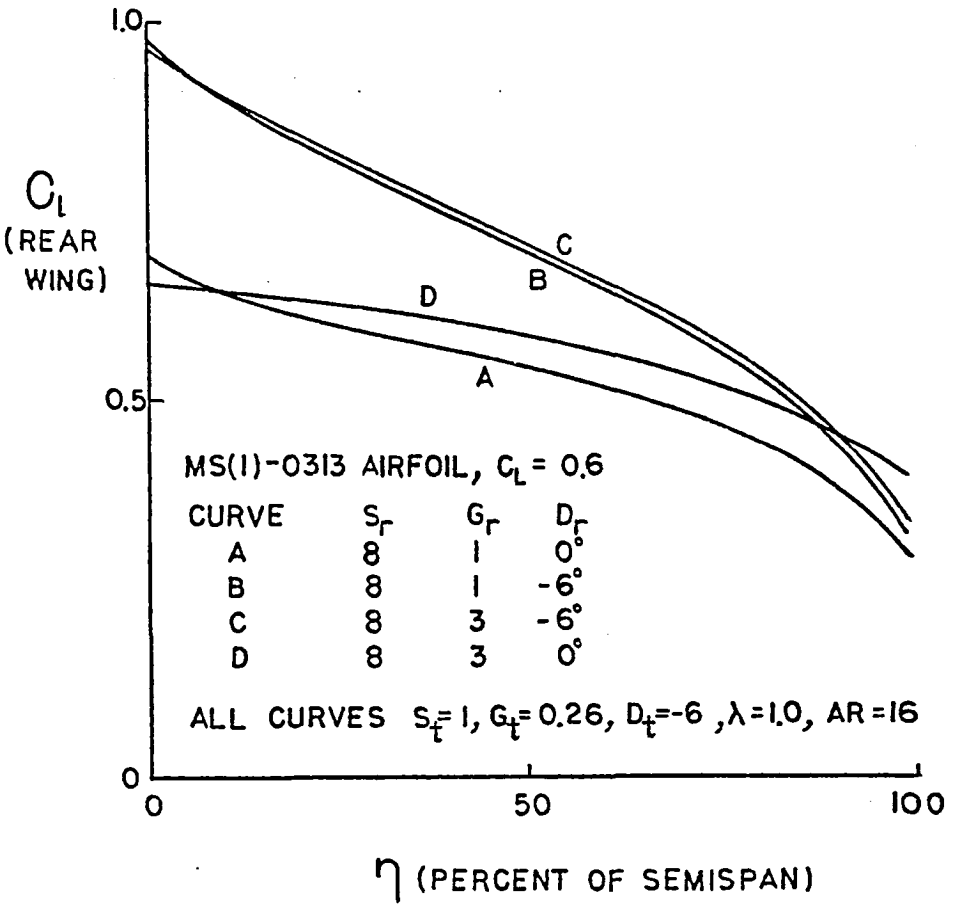

Figure 30. Rear Wing Span Lift Distribution for Gap and Decalage Variations.

lift distribution. A G = 3 was chosen so that the front wing could be on top of the fuselage with the rear wing on the bottom of the fuselage. A taper ratio of 1.0 yielded the least induced drag. This is because the wing was optimized for a taper ratio of one and at taper ratios then less than one the outer wing would be at a higher loading. For the final SFSR wing placement cross flow instability calculations after Beasley[35] were conducted. These calculations verified that cross flow instability did not exist for the cruise flow conditions investigated.

The optimization results for the SFSR are shown in Figure 31 compared with the baseline.

The SFSR configuration was not designed for lateral stability. Lateral stability requirements could cause the necessity of a larger vertical tail and changes in wing dihedral which would raise the drag and lower the range.

STRUCTURES

Introduction

At the start of the present study it was recognized that the main effort in structural analysis should be concentrated on the estimation of weight for the wing systems of current interest. Other structural systems for the present aircraft were considered to be more or less conventional and, thus, adequately dealt with using available published weight estimating formulas. It was recognized, however, that these wing systems could lead to reduced fuselage bending moments and could, therefore, permit lighter fuselage structure, but the use of existing formulas was to be conservative and suitable within the time constraints.

The need for quality weight estimates for the present wing systems posed a problem, since formulas available for the weight estimation of conventional monoplane wings, however manipulated or adjusted, could not be said to be

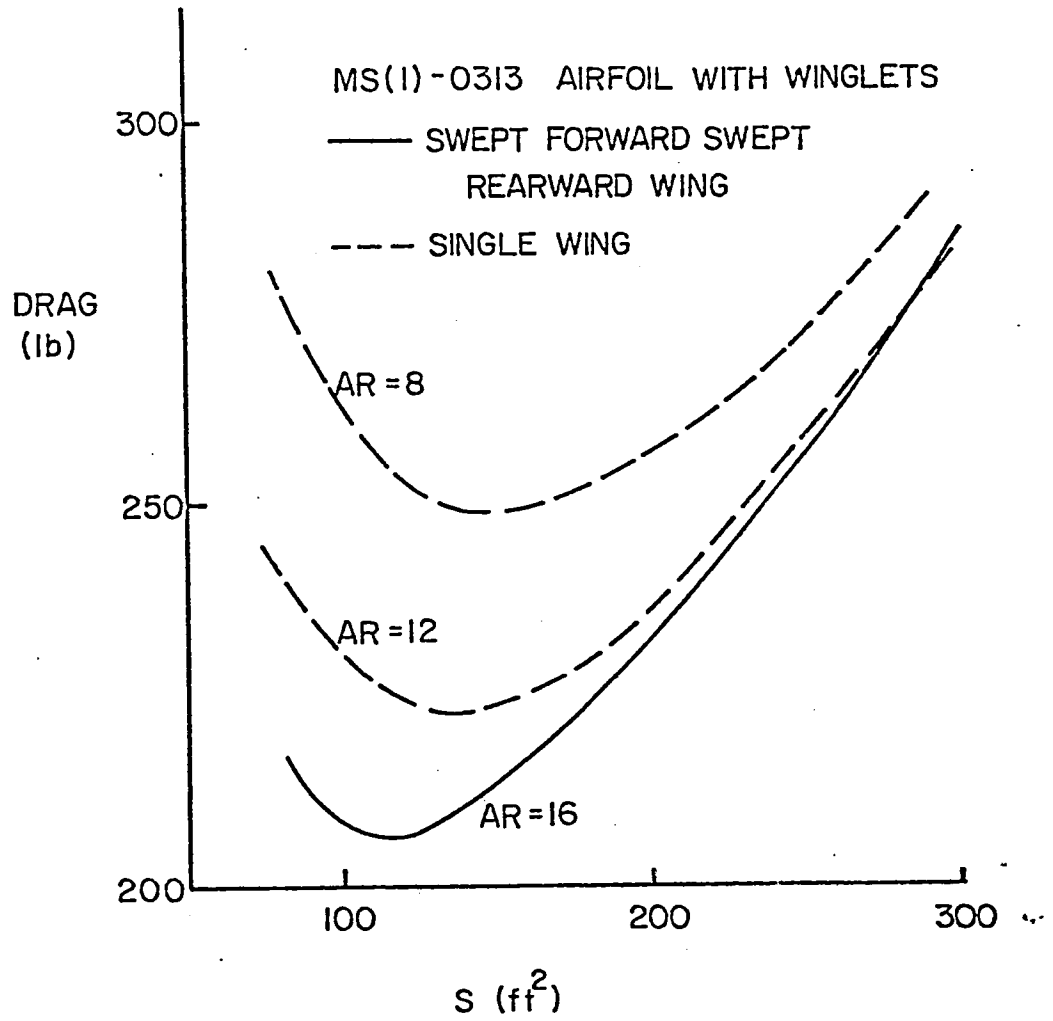

Figure 31. Trim Drag Optimization Results for the SFSR Configuration.

appropriate for the task. According to Torenbeek[3], for example, between 50 and 70 percent of the weight of a conventional wing is attributable to structure specifically intended to react out-of-plane bending loads. Only a small portion of the remaining weight (in the neighborhood of 10 percent) is attributable to structure intended to react torsion. The residual weight is either non-structural or required to react loads which are not the subject of this study, e.g., landing loads, flap loads, etc.

Owing to the geometry of the wing configurations of present interest, normal cruise loading may produce considerable in-plane bending loads and considerable torsional loading in conjunction with out-of-plane bending loads. The loading picture is further complicated by intermediate structural connections between the wings and the load discontinuities these connections introduce.

In view of the above, it was concluded that the only valid approach to weight estimation was to design the wing system structurally to safely react limiting loads, to optimize the structure subject to the constraint that it remain viable for the specified loading, and then to estimate its weight. A methodology was developed to perform these tasks. It is described in the following section.

Having established the needed methodology, wing weights were determined for the baseline, dual wing, and swept forward swept rearward configurations both for the six-place and the twelve-place payloads.

Although time and resources were limited, the various wing system models developed for the above purpose were additionally subjected to preliminary modal analyses in order to identify possible dynamics problems and were also subjected to a limited parameter survey in order to explain better how they function structurally.

Structural Model

The weight estimation for the wing systems of present interest must basically

begin with a procedure for appropriately sizing the wing structure. The sizing criteria employed in this paper are based upon producing a "fully stressed structure," i.e., a structure having all members either stressed to limiting stress levels or of specified minimum dimensions, when the structure is influenced by design limiting loads.

The generation of a fully stressed structure requires an analysis to determine stresses in all the members in the wing system. Due to the static redundancy of the dual wing configurations studied here, a method for determining the loads carried by each wing is required before a stress analysis of structural elements may be performed for the individual wings.

The first step, therefore, in the weight estimation procedure is to model the entire wing configuration for assumed reasonable element properties, to subject it to the design limiting load, and to determine the load distribution on each wing. The loads thus determined are then used to size the members of the wing configuration based upon a fully stressed structure design procedure. This constitutes the second step in the weight estimation procedure. Alterations in member properties, however, change the nature of load sharing between the wings. The steps described above must be repeated using the modified structure properties obtained from the previous iteration until the results converge to within an acceptable tolerance.

The first step of the weight estimation procedure is the execution of a program PREPROCESSOR, which generates a NASTRAN data deck for the wing configuration of interest using simple beam elements (CBAR). A single beam element is placed between two adjacent stations along the span.

Wing structure for the purpose of this study is considered to be an assemblage of longitudinal stiffeners (stiffeners, spar caps and/or longerons) and longitudinal webs (skins, spar webs and keel beams). The sectional properties of the appropriate beam element are thus calculated using the average of the cross

sectional properties for the web-stiffener structure at two adjacent spanwise stations.

PREPROCESSOR accepts as input the geometry of the given wing configuration along with estimates for stiffener areas and web thicknesses. Each wing is modelled with beam elements along the elastic axis.

The elastic axis is assumed to be the axis connecting the shear centers of spanwise stations. Due to varying element properties along the span, the shear centers of spanwise stations do not lie on a straight line. Linear regression is used to fit an elastic axis passing through the shear centers in the mid-chord plane of the wing.

Rigid elements (CRIGD1) connect the leading and trailing edges at each station. Plot elements (PLOTEL) connect the grid points along the leading and trailing edges of the wings. Although the present concern is with stresses rather than deflections, the use of rigid elements permits the determination of deflections of the leading and trailing edges from the NASTRAN static analysis. These deflections may be important in the aerodynamics of closely-coupled wings and are available for comparison to permissible values.

In the cases of wings having connections other than tip connections, the connections between wings are made at appropriate span locations on the elastic axis of each wing.

The input for the NASTRAN beam model consists of loads due to aerodynamic forces and moments, and those due to the weight of the structure. This input is multiplied by an appropriate factor of safety and by an appropriate load factor. Local values along the span for the lift coefficients, sectional lift curve slopes, sectional zero lift coefficients, angles of attack and pitching moment coefficients give the magnitudes and locations along the chord of the lift forces and pitching moments. These forces are applied at the grid points of the structural model which are connected by rigid elements to those on the elastic axis.

The weight of the wing provides an inertia relief. The center of mass, weight of each bay and the moments of inertia of each bay are calculated by PREPROCESSOR. This information is used to prepare an inertial property data card for each bay in the appropriate NASTRAN format.

The NASTRAN static analysis output provides the forces in the CBAR elements for each wing. The next step in the weight estimation procedure is the execution of the program BIFORCE which simply processes the bending moments, torques and axial forces in the CBAR elements to generate station loads for each wing.

The program BISTRESS, the execution of which follows the above step in the weight estimation procedure, uses these loads to generate areas and thicknesses for structural elements in the wing configuration corresponding to a fully stressed structure. The internals of BISTRESS are illustrated in Figure 32. The geometry of the wing configuration, the bending moments, torques and axial loads at each station along with the estimate for the web thicknesses and stiffener areas used in the preceding NASTRAN run are input to BISTRESS. The stress analysis for the wing configuration is carried out using SEMOBEAM, a program by Cook[36].

SEMOBEAM assumes a semi-monocoque wing structure consisting of axial force members (stiffeners) and shear panels (webs). The displacement formulation is used to calculate the stiffener axial stresses and the web shear stresses. Although the method for calculating stresses employed by SEMOBEAM lacks the generality of a more detailed finite element analysis, it provides sufficient accuracy for preliminary design procedures and is inexpensive to run.

SEMOBEAM thus gives the stresses in the wing members for particular values of stiffener areas, web thickness and wing loads. An iterative procedure is used to size the wing structure for a set of loads to obtain a fully stressed structure.

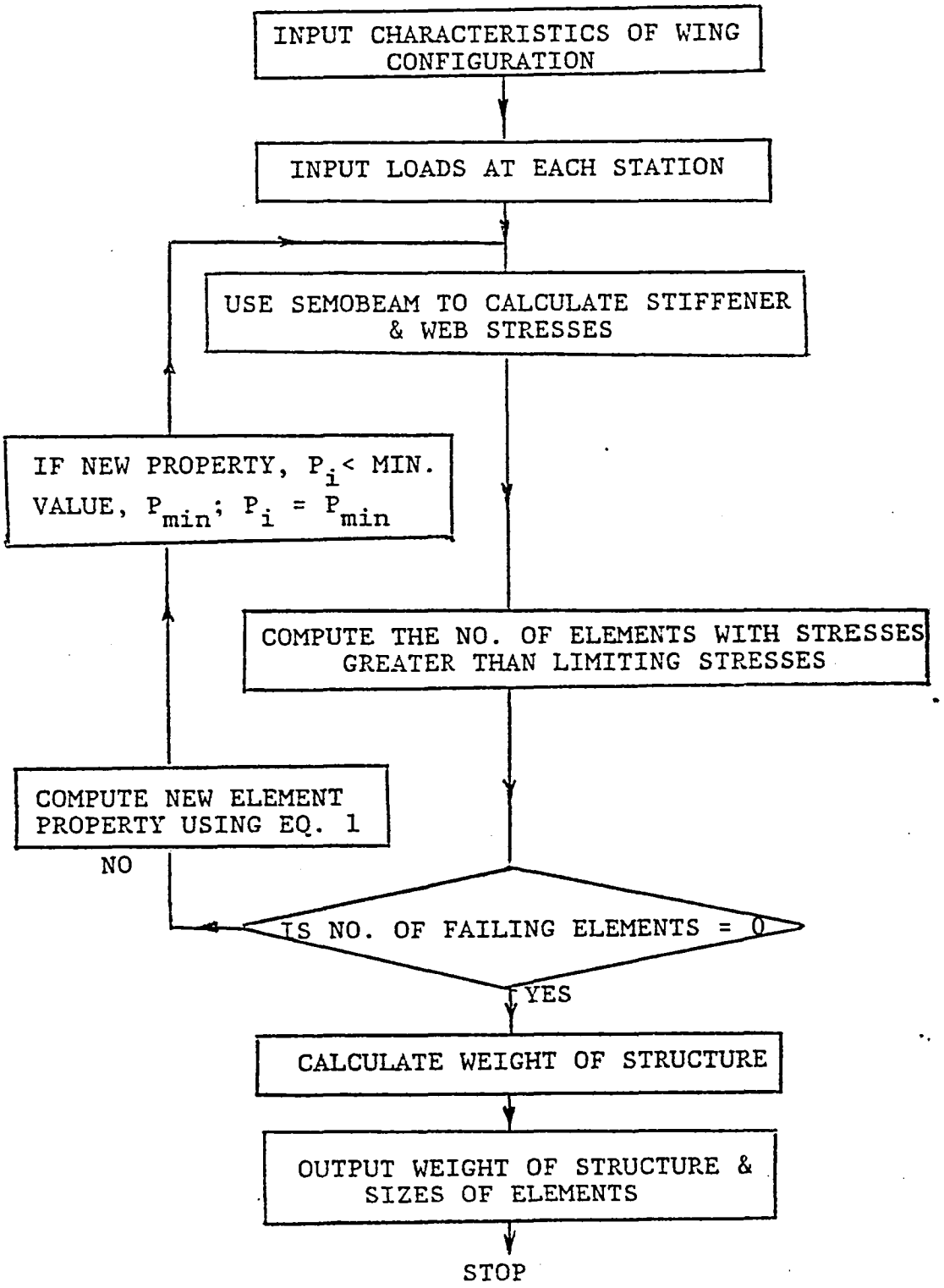

Figure 32. Flowchart for the BISTRESS Program.

The webs and spars were evaluated for buckling as well as for shear failure. Timoshenko's formula for buckling of continuously supported rectangular plates loaded at the edge by pure shear[37] is used. The value of the critical shear stress is in general different for different spar webs and skin panels within the structure. The BISTRESS program was set up to accept a single value for the limiting shear stress in webs. The value of τ_{cr} for the web with the smallest value of $k(t/b)^2$ was calculated and used as the limiting value.

The BISTRESS program calculates the weight of the wing structural box using values for the web thicknesses and stiffener areas obtained after suitable convergence.

The sequence of these programs is executed until the difference in weight generated by two consecutive BISTRESS runs is within an acceptable tolerance indicating that the process of mass distribution on the wing structure has converged.

In order to avoid confusion and subjective assessments, all of the present work is based upon the use of a conventional aircraft structural material -- 7079 Alclad aluminum. As reported in Ref. (1), the use of composites for wing structure should yield a wing weight which is 75% of the aluminum weight. In a more recent and, perhaps, more authoritative reference[38] it is stated that a composite wing structure which weighs 63% that of the structurally equivalent aluminum wing is possible. Where we have quoted composite weights in the following, we have assumed the 37% weight reduction relative to our aluminum models.

Each of our structural models is based upon the MS(1)-0313 airfoil. The structural box is assumed throughout to have its forward spar at 15% of chord and its aft spar at 75% of chord. The chordwise internal construction of the structural box used for all of the present wing systems is illustrated in Figure 33.

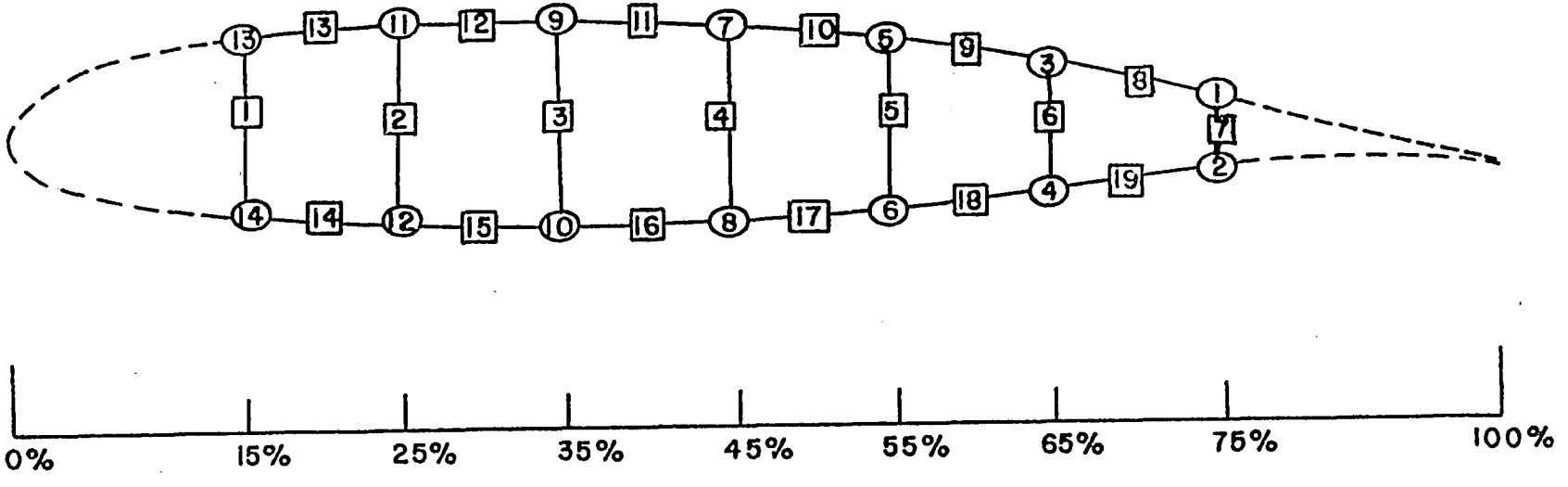

Figure 33. Structural Box using the MS(1)-0313 Airfoil.

The weight estimation procedure described in the previous section produces an estimate of the weight of the structural box only. To this weight we have added in each case the weight of an aluminum leading edge assumed to be 2.5 mm (0.1 in.) thick and the weight of a trailing edge assumed to be 0.76 mm (0.03 in.) thick. Also included in our weight estimation is a winglet weight estimation which is based upon simple scaling by surface area and the results of a study by Gifford and van Dam[39]. Structure required to support the winglet and additional structure required to tie the wings together is also included in the various models.

The loads used to design the present structure associate with cruise and maximum cruise weight. Inertia relief is incorporated. A factor of safety of 1.5 has been employed and a load factor of 3.8 for vertical loading is used. The latter factor is quoted in the FAR's for aircraft weighing less than 1900 kg (4200 lbs.) and is thus appropriate for the six-place aircraft of interest. Since this factor has also been used here for the twelve-place aircraft, our weight estimates for the latter aircraft are considered to be quite conservative.

In order to illustrate the credibility of the present approach, Torenbeek's weight estimating equation (3) was applied to the present conventional six-place wing. The predicted weight based upon this formula is 2,868 N (1420 lbs.) without winglets. The weight estimate for the conventional six-place wing determined by the present approach is 1,806 N (406 lbs.) -- this includes the leading and trailing edges and does not include winglets.

The primary results of the present investigation are summarized for the six-place configurations in Table 9 and in Table 10 for the twelve-place configurations. Shown in the first line of each figure is the structural box weight for the various configurations. These weights were developed by the weight estimation procedure described in the previous section. Clearly seen

TABLE 9.

WEIGHT BREAKDOWN FOR THE SIX-PLACE WING SYSTEMS

	CONVENTIONAL N (lbs.)	DUAL WING N (lbs.)	SWEPT FORWARD SWEPT REARWARD N (lbs.)
Structural Box	2,448 (550.3)	1,744 (392.0)	1,887 (424.3)
Horizontal Tail	139 (31.3)	139 (31.3)	---
Ties	---	205 (46.0)	76 (17.0)
Winglets	173 (39.0)	124 (28.0)	142 (32.0)
Leading & Trailing Edges	248 (55.7)	462 (104.0)	285 (64.0)
TOTAL - Aluminum	3,008 (676.3)	2,675 (601.3)	2,398 (537.3)
TOTAL - Composite	1,806 (406)	1,419 (319)	1,503 (338)

TABLE 10.

WEIGHT BREAKDOWN FOR THE TWELVE-PLACE WING SYSTEMS

	CONVENTIONAL N (lbs.)	DUAL WING N (lbs.)	SWEPT FORWARD SWEPT REARWARD N (lbs.)
Structural Box	3,896 (876.0)	3,403 (765.0)	3,665 (824.0)
Horizontal Tail	218 (49.0)	218 (49.0)	---
Ties	---	307 (69.0)	107 (24.0)
Winglets	307 (69.0)	240 (54.0)	267 (60.0)
Leading & Trailing Edges	488 (109.8)	912 (205.0)	560 (126.0)
TOTAL - Aluminum	4,911 (1104.0)	5,080 (1142.0)	4,609 (1036.2)
TOTAL - Composite	2,953 (664)	3,065 (689)	2,904 (652)

is that all of the dual wing systems treated in this study show a weight advantage when compared to the appropriate conventional wing insofar as the structural box is concerned. This matter will be discussed further in the concluding section of this structural write-up. Horizontal tail weights shown in the second row of each table were estimated by available formulas. Tie weights shown in the third row of each figure include intermediate struts for the biwing and wingtip structure required to couple wings in all of the dual wing configurations. Winglets weights, and leading and trailing edge weights shown in subsequent rows of each figure are determined as previously discussed. Composite weight estimates for each configuration are included in Tables 9 and 10. These are based upon the 37% weight reduction factor relative to aluminum discussed earlier in this section.

Having obtained acceptable structural models, the writers were in a position to determine other structural response quantities of interest. An acceptable structure must not only respond to limiting loads with stresses in all structural elements less than limiting stresses, but also exhibit acceptable deflections. This is particularly important in the dual wing configurations studied here where the spacing between wings and the relative angle between the wings is critical. Significant structural deflections may spoil proper aerodynamics. Shown in Table 11 are changes in the gap, stagger, and decalage for the six-place biwing, and swept forward swept rearward wing which occur when the aircraft are influenced by cruise loading. Changes are relative to the unloaded state. None of the changes shown are considered to be significant from the aerodynamic standpoint. For this reason, deflections for the twelve-place configurations were not developed and are not offered here.

Although, as has been said, there was insufficient time and resources to do a thorough investigation of the dynamics of these configurations to include

TABLE 11.

CHANGES IN GAP, STAGGER AND DECALAGE FOR SIX-PLACE AIRCRAFT IN CRUISE

	Δ GAP	Δ STAGGER	Δ DECALAGE (radians)
BIWING	-5.3028 mm	-13.9852 mm	0.3385×10^{-2}
SWEPT FORWARD SWEPT REARWARD	-16.358	-4.2722	0.1575×10^{-3}

TABLE 12.

SUMMARY OF MODAL ACTIVITY

MODE	FREQUENCY r/s (hz.)
CONVENTIONAL WING	
1st out-of-plane bending	29.4 (4.68)
2nd out-of-plane bending	166.6 (26.52)
3rd out-of-plane bending	432.0 (68.89)
BIWING	
1st out-of-plane bending	24.3 (3.86)
2nd out-of-plane bending	91.9 (14.5)
3rd out-of-plane bending	112.3 (17.9)
SWEPT FORWARD SWEPT REARWARD	
1st out-of-plane bending	31.7 (5.04)
2nd out-of-plane bending	48.1 (7.65)
3rd out-of-plane bending	66.1 (10.5)

a flutter analysis, it was believed that a quick look at modal activity was in order. The NASTRAN CBAR models had been developed during the weight estimation process and were available for this task (and for any other task that NASTRAN within the NASTRAN purview).

The first natural frequencies of vibration for the conventional six-place wing are given at the top of Table 12 for reference purposes. The assumption is that this wing is dynamically acceptable and that if the lowest natural frequencies of the dual wing configurations examined fall in the frequency range defined by those of the conventional wing (29.4 r/s to 432 r/s), then these wings too are acceptable from the dynamics standpoint. This is perhaps simplistic, but there are precedents for this approach. Owing to the increased structural complexity of the dual wing configurations studied, one would expect and does observe an increased number of natural frequencies in a given frequency band. Given then in Table 12 are the three lowest natural frequencies for the six-place biwing, swept forward swept rearward and joined wing. Seen is that the lowest natural frequency for each configuration examined associates with out-of-plane bending and has a value which is comparable to that of the conventional wing. It certainly deserves further study, but based upon the present work, one may observe that these dual wing configurations manifest no pathological dynamic behavior and that they may be as dynamically suitable as the conventional wing.

Torsional natural frequencies were also determined for these configurations. The first torsional frequency of the baseline is 929 r/s. Considerably lower values were determined for the dual wing and the swept forward swept rearward wing system -- these are 226 r/s and 60 r/s, respectively.

The complexity of the dual wing structures studies led to questions concerning how their weight depended upon overall geometry. The methodology for

weight estimation described in the previous section was used as a tool to conduct a limited parameter study involving geometric variations for the six-place dual wing configurations of interest. The span, the average chord and the relative disposition of the two wings were the parameters chosen for this study. The relative disposition of the two wings is described here by the angle θ which is defined in Fig. 34.

The parameters in the above study were varied independently to span the range which included the design values of the parameters for the three six-place dual wing configurations. Thus the wing span was varied from 11.278 m (37.00 ft) to 13.148 m (43.14 ft), the average chord from 0.352 m (1.15 ft) to 0.410 m (1.34 ft), and the angle θ from 14° to 28°.

It is the structure and its weight that are of interest here. No claim is made for the aerodynamic efficiency of a given configuration produced during this parameter study. Loading has adjusted so that net lift was the same for all variations of the biwing, for all variations of the swept forward swept rearward. In each case local lift coefficients were adjusted to preserve (approximately) the lift force distribution of the original configuration, that is, the configuration characterized in Table a1 and by circles on the following illustrations.

Figures 35 through 37 show the structural weights produced during this parametric study. The structural weight is seen to increase with an increase in span and a decrease in chord for all configurations. An increase in the angle θ reduces the structural box weight for the two wing systems as seen in Fig. 39.

Figure 35 shows the results of the span variation. For a given span the swept forward swept rearward configuration is lighter than the dual wing.

Figure 36 shows the dual wing configuration to be the lightest of the three for a given chord. The sensitivity to weight increase with increasing chords is the same for both configurations.

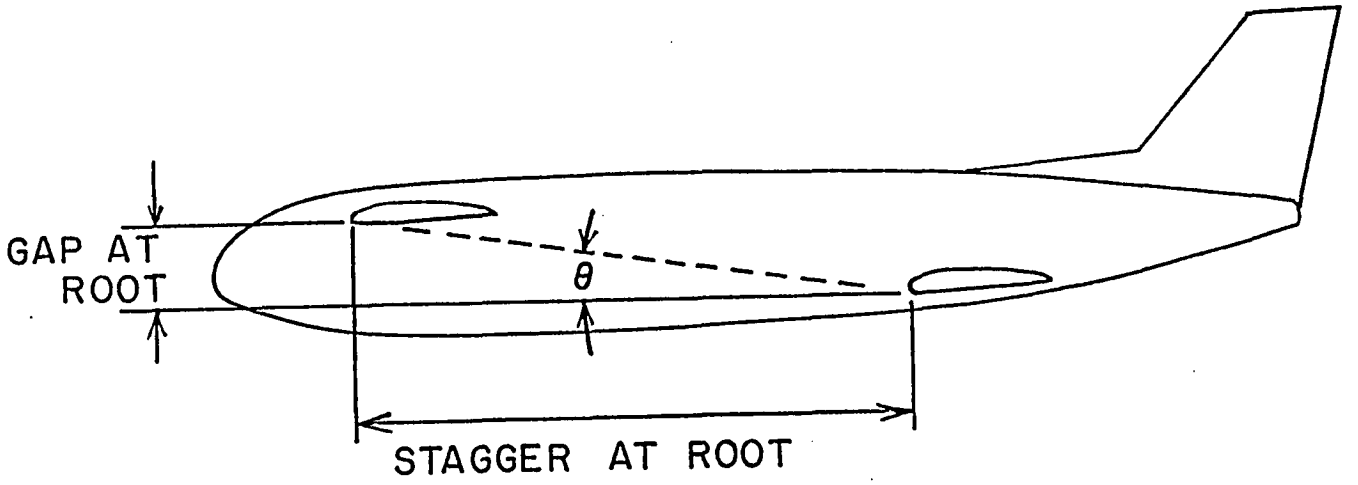

Figure 34. The angle θ.

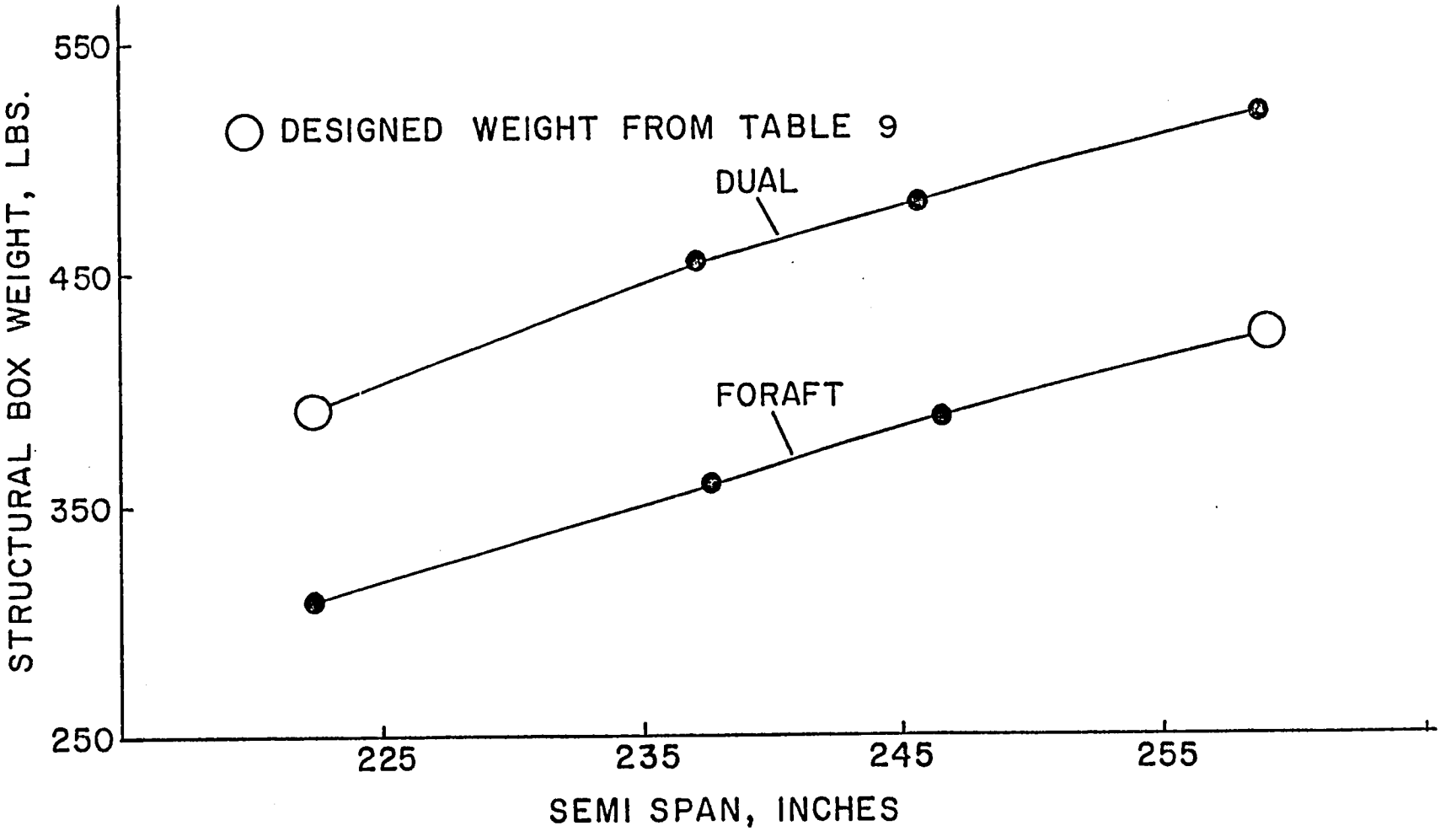

Figure 35. Structural Box Weight vs. Semi Span for Six-Place Configurations.

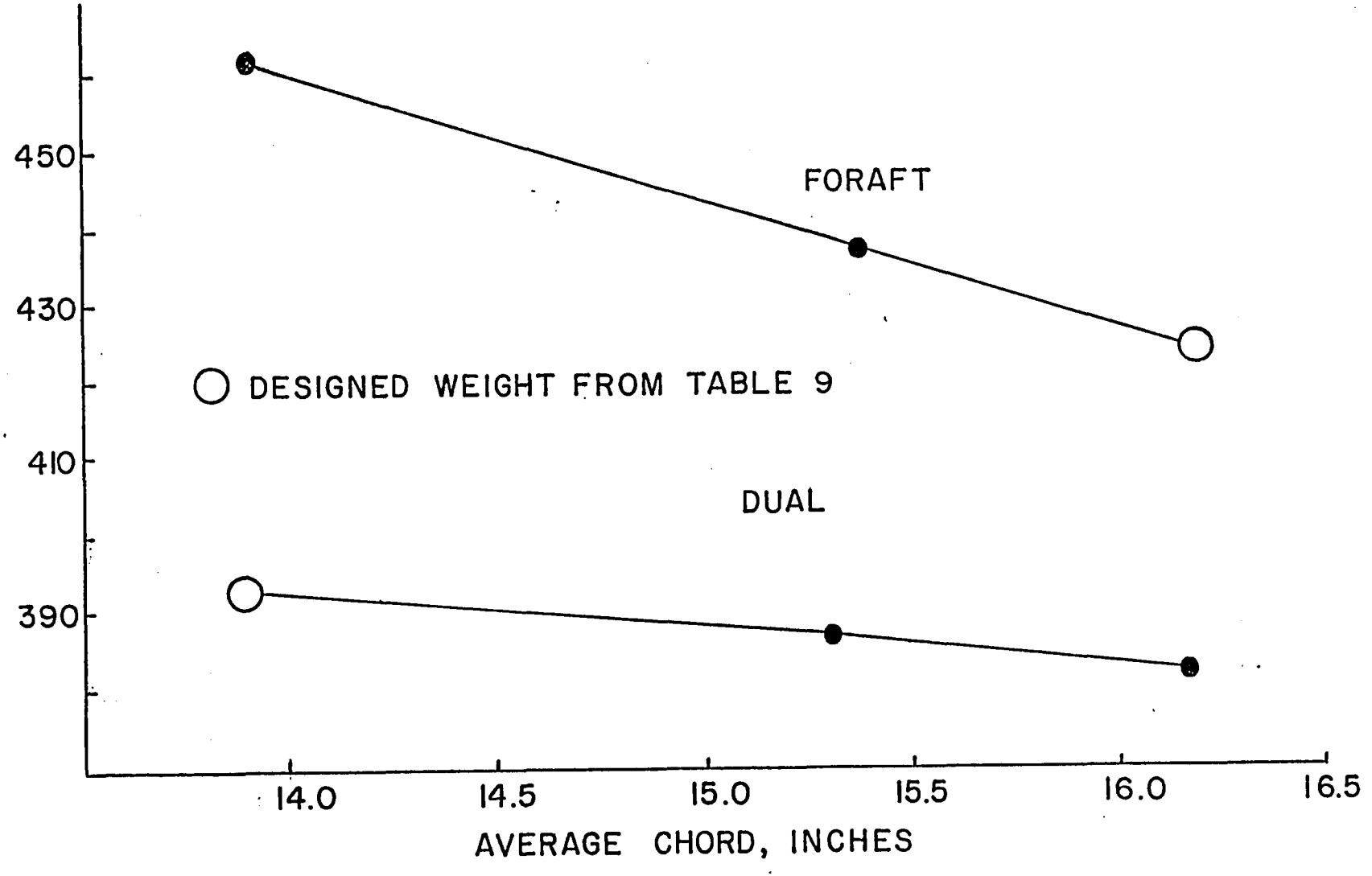

Figure 36. Structural Box Weight vs. Average Chord for Six-Place Configuration.

Figure 37 shows the weight of the swept forward swept rearward configuration to be strongly influenced by the angle θ for values of θ greater than 25°. For a given θ the biwing is the lightest.

Discussion

The weight estimation procedure described herein functions accurately and effectively. It is fast, inexpensive and well-suited to the needs of preliminary design. Based upon our examination of the open literature, the procedure appears to be a unique methodology for designing and estimating the weight of fairly general dual wing configurations. The resulting structural models are well-suited to a variety of other analysis tasks as illustrated in the previous section by the modal analysis and the "quick-look" parameter study.

We have described the wings produced by the procedure as structurally optimal. This is almost true for a class of wings having the internal structure shown in Fig. 33 and structural box chordwise size described in the previous section, i.e., forward spar at 15% of chord and aft spar at 75% of chord. There is no reason to believe that another internal structure might not have been better for one or several of the wing configurations examined. In addition, time did not permit an adequate study of the influence on weight of structural ties between the wings, nor was there time to examine the matter of optimal placement of these ties.

One element of conservatism built into the procedure developed for this study had to do with the application to the entire wing of a buckling criterion based upon the web having the smallest $k(t/b)$. Insofar as study results are concerned, this criterion, in conjunction with the hypothesized internal structure of the structural box, tended to make the twelve-place dual wing and swept forward swept rearward results relatively heavy both with respect to six-place

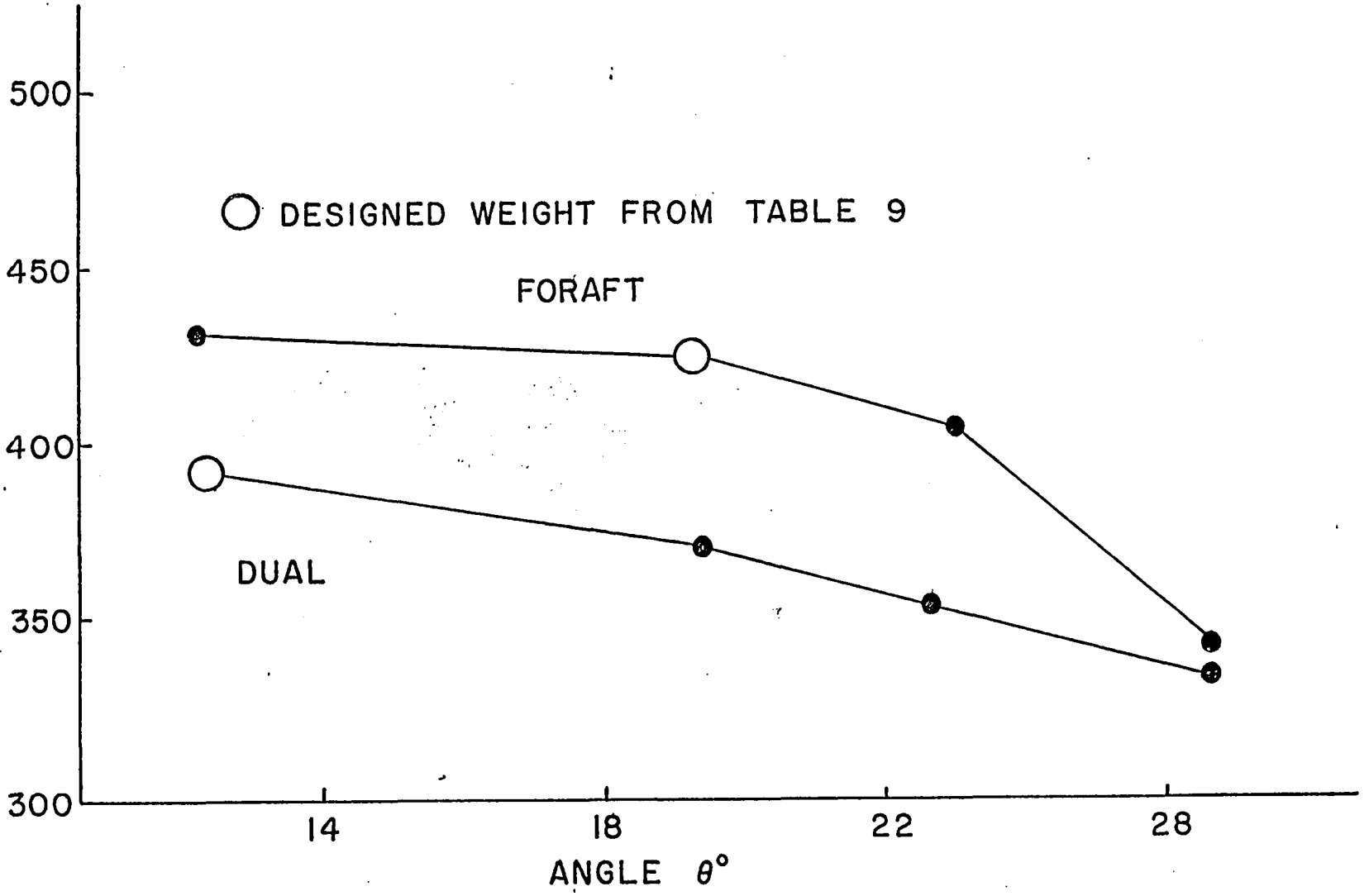

Figure 37. Structural Box Weight vs. Angle θ for Six-Place Configurations.

results and with respect to the conventional twelve-place wing. The structural box weight of the six-place baseline is 1.4 times the structural box weight for the six-place dual. The structural box weight for the twelve-place baseline is however only 1.1 times the structural box weight of the twelve-place dual. This higher weight estimated for the twelve-place dual as compared to the six-place dual is due to the fact that the same structural box layout is used for all these wings.

The root chord for the six-place baseline is 3.2 times the root chord for the six-place dual whereas the root chord for the twelve-place baseline is 1.5 times the root chord for the twelve-place dual. Since the same structural box layout is used the stiffeners and webs are located at the same chordwise position for all the wing systems studied. The higher chord of the twelve-place dual as compared to the six-place dual implies that the webs in the twelve-place dual are broader which leads to lower permissible buckling stress and a higher weight.

All of the dual wing configurations produced during this study for the six-place aircraft are significantly lighter than the six-place conventional wing -- most notably, the swept forward swept rearward wing system offers a weight advantage of 63 kg (139 lbs.) in aluminum and 40 kg (88 lbs.) in composite materials. Concerning what are considered to be the least subjective results -- structural box weights -- all dual wing configurations offer quite significant weight reduction possibilities relative to the conventional wing: 30% in aluminum for the dual wing, 23% in aluminum for the swept forward swept rearward, and 20% in aluminum for the joined wing.

For the twelve-place dual wing configurations produced during this study, the structural boxes are lighter than that of the conventional twelve-place wing: 50 kg (111 lbs.) in aluminum and 32 kg (70 lbs.) in composites for the biwing, and 24 kg (52 lbs.) in aluminum and 15 kg (33 lbs.) in composites for

the swept forward swept rearward wing configuration. It is believed that a redesign of the structural boxes for both the twelve-place dual wing configurations and the repair to the web buckling criterion discussed above will result in larger weight reductions for the twelve-place dual wing configurations relative to the twelve-place conventional wing.

In summary, it appears possible for the present applications to build a relatively light dual wing system in either aluminum or composite material. These dual wing systems appear to perform adequately from the standpoints of both statics and dynamics. The design of these systems will be more complicated -- requiring, even in the preliminary stages, more computer analysis and less reliance on proven formulas and established strategies. Based upon the present results it is concluded that the additional complexity -- both in terms of structure and design -- is worthwhile.

REFERENCES

1. Nicolai, L. M., Fundamentals of Aircraft Design, METS, Inc., San Jose, Calif., 1975, pp. 5.1-5.24, pp. 20.1-20.24.

2. Torenbeek, E., Synthesis of Subsonic Airplane Design, Delft University Press, 1976, pp. 27-76, pp. 263-302, p. 352.

3. Torenbeek, E., "Prediction of Wing Group Weight for Preliminary Design," Aircraft Engineering, July 1971.

4. Hayes, B., Lopez, R., and Rhodes, M., "General Aviation Light Turbo-Powered Aircraft," UMR Senior Design Project, 1980.

5. Selberg, B. and Cronin, D. L., NASA Semi-Annual Progress Report, NASA Grant NAG1 26, 1981.

6. Kohlman, D. L. and Holmes, B. J., "Assessment of Advanced Technologies for High Performance Single-Engine Business Airplanes," 13th ICAS/AIAA Aircraft Systems and Technology Meeting, Paper No. ICAS-82-1.4.3, August 1982.

7. Holmes, B. J. and Croom, C. C., "Aerodynamic Design Data for a Cruise-Matched High Performance Single Engine Airplane," SAE Paper 810625, 1981.

8. Benstein, E. H. and Smith, R., "Advanced General Aviation Turbine Engine (GATE) Study," NASA CR-159624, 1979.

9. Anon., Evaluation of Torenbeek's weight estimating formula for a range of aircraft wings, NASA-ARC.

10. Rokhsaz, K., "Analytical Investigation of the Aerodynamic Characteristics of Dual Wing Systems," UMR Thesis, Rolla, Mo., 1980.

11. Thwaites, B., "Approximate Calculation of the Laminar Boundary Layer," Aero. Quarterly I, 1949.

12. Michel, R., "Etude de la Transition sur les Profiles d'Aile; Establissement d'un Critere de Determination de Point de Transition et Calcul de la Trainee de Profile Incompressible," ONERA Rept. 1/1578A, 1951.

13. Cebeci, T. and Bradshaw, P., Momentum Transfer in Boundary Layers, Hemisphere Publishing Corp., Washington, 1977, pp. 192-194.

14. Cebeci, T. and Smith, A. M. O., "Calculation of Profile Drag of Airfoils at Low Mach Numbers," Journal of Aircraft, Vol. 5, Nov.-Dec., 1968, pp. 535-542.

15. McGhee, R. J., "Wind Tunnel Results for a 13-Percent-Thick Medium Speed Airfoil Section," NASA TP-1498, 1981.

16. Somers, D. M., "Design and Experimental Results for a Flapped Natural-Laminar-Flow Airfoil for General Aviation Applications," NASA TR-1865, June 1981.

17. Tulinius, J., "Unified Subsonic, Transonic, and Supersonic NAR Vortex Lattice," TFD-72-523, North American Rockwell, Los Angeles, 1972.

18. Paulson, J. W., "Application of Vortex Lattice Theory to Preliminary Aerodynamic Design," National Aeronautics and Space Administration, Langley Research Center, Langley Station, Va., 1976.

19. Roskam, J., Methods for Estimating Drag Polars of Subsonic Airplanes, published by the Author, Lawrence, Kansas, 1971, p. 2.3.

20. Hoerner, S. F., Fluid Dynamic Drag, published by the Author, 1965, pp. 6.15-6.19.

21. Crawford, D. R., A Practical Guide to Airplane Performance and Design, 1st ed., Crawford Aviation, Torrance, Calif., 1979, p. 174.

22. Whitcomb, R. T., "A Design Approach and Selected Wind-Tunnel Results at High Subsonic Speeds for Wing-Tip Mounted Winglets," NASA TN D-8260, 1976.

23. Roskam, J., Methods for Estimating Stability and Control Derivatives of Conventional Subsonic Airplanes, published by the Author, Lawrence, Kansas, 1971, pp. 21. - 12.2.

24. Roskam, J., Airplane Flight Dynamics and Automatic Flight Controls, Part I, Roskam Aviation and Engineering Corp., 1979, pp. 243-377.

25. Keith, M. W., "Parametric Canard/Wing Aerodynamic Tradeoff Analysis and Trim Design Comparison of Canard and Conventional High Performance General Aviation Configurations," UMR Thesis, Rolla, Mo., 1981.

26. Norton, F. H., "Effect of Staggering a Biplane," NACA TN-710, 1918.

27. Knight, and Noyes, R. W., "Wind Tunnel Test on a Series of Biplane Wing Models, Part I. Effects of Changes in Stagger and Gap," NACA TN-310, 1929.

28. Knight, and Noyes, R. W., "Wind Tunnel Tests on a Series of Biplane Wing Models, Part II. Effects of Changes in Decalage, Dihedral, Sweepback, and Overhand," NACA TN-325, 1929.

29. Knight, and Noyes, R. W., "Wind Tunnel Tests on a Series of Biplane Wing Models, Part III. Effects of Changes in Various Combinations of Stagger, Gap, and Decalage," NACA TN-330, 1929.

30. Nenadovitch, M., "Recherches sur les Cellules Biplane Rigides d'Envergure Infine," Publications Scientifiques et Techniques du Minister de L'Air, Institut Aero'-technique de Saint-Cyr, Paris, 1936.

31. Olson, E. C. and Selberg, B. P., "Experimental Determination of Improved Aerodynamic Characteristics Utilizing Biplane Wing Configurations," Journal of Aircraft, Vol. 13, April 1976, pp. 256-261.

32. Prandtl, L. and Tietjens, O. G., Applied Hydro- and Aero-mechanics, Dover Publications, Inc., New York, 1957, pp. 213-216.

33. Rhodes, Mark D., "Advantages of Dual Wing Aircraft Designs," UMR Thesis, Rolla, Mo., 1982.

34. Vincent, Gary D., "Aerodynamics of Closely Coupled Wings for Varying Chords and Airfoil Planforms," UMR Thesis, Rolla, Mo., 1982.

35. Beasley, J. A., "Calculation of the Laminar Boundary Layer and Prediction of Transition on a Sheared Wing," R.A.E. Report No. 3787, October 1973.

36. Cook, E. L., "Semimonocoque Beam Analysis: A Displacement Formulation," Society of Automotive Engineers, SAE Paper 740385, July 1974.

37. Timoshenko, S., Theory of Elastic Stability, First Edition, McGraw-Hill, 1936, Chapter 17.

38. Lange, R. H., et al., "Feasibility Study of the Transonic Biplane Concept for Transport Aircraft Applications," NASA CR-132462, June 1974.

39. Gifford, R. V. and van Dam, C. P., "The Design Integration of Wingtip Devices for Light General Aviation Aircraft," ICAS-82-1.4.4, October 1982.

1. Report No.	2. Government Accession No.	3. Recipient's Catalog No.
NASA CR-172529		

4. Title and Subtitle	5. Report Date
AERODYNAMIC-STRUCTURAL STUDY OF CANARD WING, DUAL WING, AND CONVENTIONAL WING SYSTEMS FOR GENERAL AVIATION APPLICATIONS	February 1985
	6. Performing Organization Code

7. Author(s)	8. Performing Organization Report No.
Bruce P. Selberg and Donald L. Cronin	
	10. Work Unit No.

9. Performing Organization Name and Address	11. Contract or Grant No.
University of Missouri-Rolla Mechanical & Aerospace Engineering Department Rolla, MO 65401	*NAG1-26*
	13. Type of Report and Period Covered
12. Sponsoring Agency Name and Address	*Contractor Report*
NASA Langley Research Center *Hampton, VA 23665*	14. Sponsoring Agency Code
	505-45-43-02

15. Supplementary Notes

Langley Technical Monitor: Bruce J. Holmes
Final Report

16. Abstract

An analytical aerodynamic-structural airplane configuration study was conducted to assess performance gains achievable through advanced design concepts. The mission specification was for 350 mph, range of 1500 st. mi., at altitudes between 30,000 and 40,000 ft. Two payload classes were studied - 1200 lb (6 passengers) and 2400 lb (12 passengers). The configurations analyzed included canard wings, closely coupled dual wings, swept forward - swept rearward wings, joined wings, and conventional wing tail arrangements.

The results illustrate substantial performance gains possible with the dual wing configuration. These gains result from weight savings due to predicted structural efficiencies. The need for further studies of structural efficiencies for the various advanced configurations was highlighted.

17. Key Words (Suggested by Author(s))	18. Distribution Statement
General aviation *Advanced configurations* *Canard* *Dual wing* *Joined wing* *Laminar flow*	*Unclassified - unlimited* Subject Category 02

19. Security Classif. (of this report)	20. Security Classif. (of this page)	21. No. of Pages	22. Price
unclassified	*unclassified*	86	A05

For sale by the National Technical Information Service, Springfield, Virginia 22161